LBL-1840
c.1

PAIR-QUASIPARTICLE POTENTIAL DIFFERENCES IN CURRENT-CARRYING SUPERCONDUCTORS

James Lenander Paterson
(Ph. D. Thesis)

July 1973

Prepared for the U.S. Atomic Energy Commission
under Contract W-7405-ENG-48

For Reference

Not to be taken from this room

LAWRENCE BERKELEY LABORATORY
UNIVERSITY OF CALIFORNIA
BERKELEY

LBL-1840
c.1

DISCLAIMER

This document was prepared as an account of work sponsored by the United States Government. While this document is believed to contain correct information, neither the United States Government nor any agency thereof, nor the Regents of the University of California, nor any of their employees, makes any warranty, express or implied, or assumes any legal responsibility for the accuracy, completeness, or usefulness of any information, apparatus, product, or process disclosed, or represents that its use would not infringe privately owned rights. Reference herein to any specific commercial product, process, or service by its trade name, trademark, manufacturer, or otherwise, does not necessarily constitute or imply its endorsement, recommendation, or favoring by the United States Government or any agency thereof, or the Regents of the University of California. The views and opinions of authors expressed herein do not necessarily state or reflect those of the United States Government or any agency thereof or the Regents of the University of California.

0 0 0 0 3 9 0 0 7 5 2

PAIR-QUASIPARTICLE POTENTIAL DIFFERENCES IN CURRENT-CARRYING SUPERCONDUCTORS

Contents

ABSTRACT v

I. INTRODUCTION 1

II. THEORY 7

III. EXPERIMENTAL METHODS 20

A. Sample Preparation for Tin Samples 20

B. Sample Preparation for Lead Samples 23

C. Shielding 24

D. Electronics 26

E. Noise and Sensitivity 28

F. Measurements 30

IV. EXPERIMENTAL RESULTS - TIN 32

A. The Injection Junction 32

B. Probe Junction 34

C. Determination of τ_Q 36

D. The Voltage and Temperature Dependences of F 42

V. EXPERIMENTAL RESULTS - LEAD 47

A. Injection Junction 47

B. Probe Junction 50

C. Comparison with Theory 50

VI. SUMMARY 55

ACKNOWLEDGMENTS 57

APPENDIX I. FEEDBACK ANALYSIS 58

APPENDIX II. ELECTRONIC PARAMETERS 63

REFERENCES 66

0 0 0 0 3 9 0 0 7 5 3

PAIR-QUASIPARTICLE POTENTIAL DIFFERENCES IN CURRENT-CARRYING SUPERCONDUCTORS

James Lenander Paterson

Inorganic Materials Research Division, Lawrence Berkeley Laboratory
and Department of Physics; University of California
Berkeley, California 94720

ABSTRACT

We have used an rf SQUID voltmeter to measure the potential difference between the quasiparticles and pairs in the current-carrying superconductors tin and lead over the temperature range 1.3K to 4.2K. The results have been compared with the theory by Tinkham which indicates that this potential difference results from a quasiparticle excitation spectrum branch imbalance or quasiparticle current in the superconductors. This branch imbalance relaxes in a characteristic time τ_Q. Our measurements for tin confirm the theoretical volume and injection voltage dependences of the nonequilibrium potential V. The temperature dependence of τ_Q is seen to be in fair agreement with the theory near T_C and in excellent agreement at low temperatures. The magnitude of τ_Q near T_C of $1 \times 10^{-10} \frac{\Delta(0)}{\Delta(T)}$ sec is in good agreement with the theoretical estimate of $2 \times 10^{-10} \frac{\Delta(0)}{\Delta(T)}$ sec and in fair agreement with the results of Clarke of $3 \times 10^{-10} \frac{\Delta(0)}{\Delta(T)}$ sec. At low temperatures the data lie below the theory by an amount which is consistent with Tinkham's estimate of $Q^*/Q \sim 0.7$ for the branch imbalance parameters. Our measurements for lead confirm the volume and injection voltage dependences of the nonequilibrium potential. The

data near 4.2K agree with Tinkham's estimate of $\tau_Q \simeq 3 \times 10^{-12}$ sec but the increase in V below 4.2K is not understood.

0 0 0 0 3 9 0 0 7 5 4

I. INTRODUCTION

The area of the response of superconductors to external stimuli has been one of considerable interest for both theorists and experimentalists. The superconductor consists of a composite system of condensed pairs (of electrons) and excited quasiparticles. If the system is perturbed from equilibrium it will return to equilibrium at a characteristic rate. The perturbation may affect the densities of the pairs and quasiparticles, the current carrying state of the pairs and quasiparticles or both.

We discuss first experiments dealing with perturbations affecting the density of pairs and quasiparticles. The thermal equilibrium density of quasiparticles n(T) in a superconductor at a temperature T is

$$n(T) = 2N(0) \int_{\Delta}^{\infty} \frac{E}{(E^2-\Delta^2)^{1/2}} \frac{1}{1+e^{E/kT}} dE, \qquad (1)$$

where N(0) is the density of states at the Fermi level per spin, $\frac{E}{(E^2-\Delta^2)^{1/2}}$ is the reduced BCS[1] density of states and $(1+e^{E/kT})^{-1}$ is the Fermi function. If this density is perturbed from equilibrium, the excess number of quasiparticles will recombine to form pairs in a characteristic time τ_R. This time has been measured using two superconducting-insulator-superconducting (SIS) tunnel junctions in series which form a system S1-I-S2-I-S3. The quasiparticles injected into S2 from S1 form a steady state excess quasiparticle density Δn which can be determined by measuring the increase in tunneling current through the S2-I-S3 probe junction. Rothwarf and Taylor[2] have indicated that the

measured lifetimes will be larger than τ_R because the phonons, created when quasiparticles recombine to form pairs, will create additional quasiparticles. They calculated the relationship between τ_{exp} and τ_R for $\Delta n \gg n(T)$ and $\Delta n \ll n(T)$. Typically, experimental values for Δn are intermediate between the low and high temperature limits of $n(T)$. For low temperatures $[\Delta n \gg n(T)]$ τ_R is independent of temperature; for higher temperatures with $\Delta n < n(T)$ the recombination rate is proportional to the number of thermally excited quasiparticles and $\tau_R \sim t^{-1/2} e^{\Delta/k_B T}$ where t is the reduced temperature T/T_C and Δ the energy gap. Gray, Long and Adkins[3] have found that for aluminum $\tau_R \sim 2 \times 10^{-6}$ sec at $\Delta/k_B T = 4$.

Owen and Scalapino[4] have shown theoretically that this excess quasiparticle density will depress the energy gap in the superconductor. Parker and Williams[5] have measured this depression of the energy gap in Sn-oxide-Sn and Pb-oxide-Pb tunnel junctions irradiated with a He-Ne laser. They observed the predicted decrease in Δ with laser power. They also measured the energy gap depression at constant laser power versus temperature and found that it saturated at low temperatures. This saturation occurs for $\Delta n = n(T)$; at still lower temperatures the quasiparticle density will be dominated by Δn and therefore independent of temperature. Since Δn is proportional to τ_R, they were able to estimate τ_R at the saturation temperature and obtain[6]

$$\tau_R^{Sn} \simeq 2 \times 10^{-9}\ T^{-1/2}\ e^{\Delta/k_B T} \qquad (\pm 50\%), \qquad (2)$$

$$\tau_R^{Pb} \simeq 2 \times 10^{-12}\ T^{-1/2}\ e^{\Delta/k_B T} \qquad (\pm \text{ factor of } 5). \qquad (3)$$

In most cases the perturbing influence on a superconductor is the current flowing through it. We turn now to a nonequilibrium condition in which the quasiparticles are carrying current in a superconductor. Measurements of the resistance of superconductor-normal metal-superconductor (SNS) junctions by Pippard, Shepherd and Tindall[7] indicated that the superconductors apparently contributed to the resistance of the junctions. This extra resistance increased with increasing temperature near the transition temperature. Rieger, Scalapino and Mercereau[8] (hereafter referred to as RSM) pointed out that there must be a transition region near a normal metal-superconductor interface in which the electron current is converted to pair current. (The electrons enter quasiparticle states in the superconductor and these quasiparticles eventually transfer their momentum to the pairs.) The time of interest in this system is the lifetime of the current-carrying quasiparticle states.

Because the condensed pairs have infinite dc conductivity (i.e. because the system is a superconductor), the gradient of the electrochemical potential of the pairs must be zero. If the pair chemical potential, which is proportional to the pair density, varies from point to point, an electrostatic potential will be established to just cancel this variation and maintain the electrochemical potential constant. If this did not occur, an infinite current would flow. For a superconductor of uniform temperature, the electrical potential of the pairs will be everywhere constant. If the quasiparticles are carrying a current, however, this current will establish a gradient in the quasiparticle electrical potential, and a difference in the

pair and quasiparticle electrical potentials will result. It is this nonequilibrium potential difference V which is measured experimentally.

The suggested RSM configuration for measuring V is shown in Fig. 1. The strip of superconductor S'-S-S_p is separated into three parts by two Josephson junctions.[9] Provided that the critical currents for these junctions are not exceeded, the pair electrical potential will be constant across the strip. The normal probe N_p, provided it carries no current (null measurement), will have the same electrical potential as the quasiparticles in S. Rieger et al. have used time-dependent Ginzburg-Landau theory for the case of a gapless superconductor S to calculate the nonequilibrium potential V and they find

$$V = \frac{I\tau}{24\, e^2 \Omega\, N(0)} , \qquad T \approx T_C , \tag{4}$$

where I is the current, τ is the Ginzburg-Landau relaxation time for the gapless case, Ω is the volume enclosed by the dashed lines in Fig. 1 which includes a depth of approximately one coherence length into the normal metal, and N(0) is the density of states per spin at the Fermi level. This potential per unit current, then, is just the resistance developed in the superconductor.

It is important at this point to emphasize that V will be nonzero only in regions of the superconductor in which the quasiparticles are carrying current. An excess quasiparticle density which carries no current will cause the chemical potentials of the pairs and quasiparticles to differ, but for this case there will be no difference in the electrical potentials V.

0 0 0 0 3 9 0 5 7 5 6

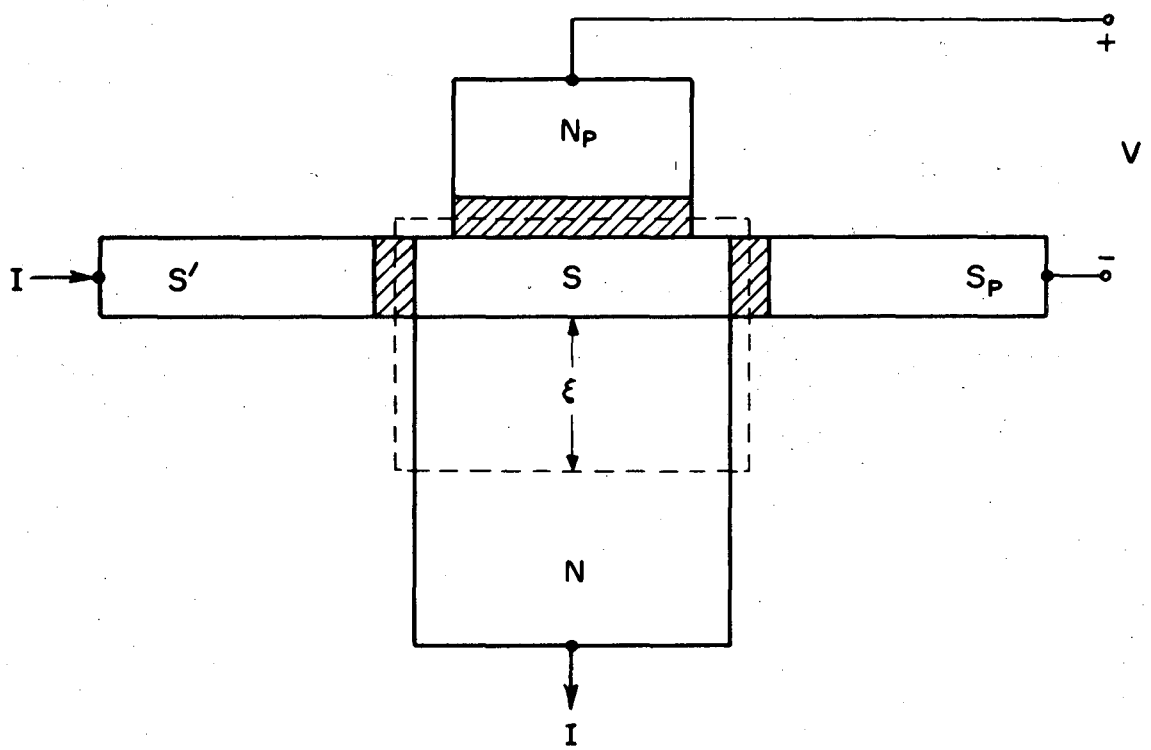

XBL 736-6343

Fig. 1. Configuration suggested by Rieger, Scalapino and Mercereau for measuring pair-quasiparticle potential difference V.

The RSM configuration has the experimental difficulty that the nonequilibrium volume is not well defined. A configuration which isolates the superconductor S and the analysis in terms of the BCS theory will be discussed in the next section. Whereas in the RSM theory the energy gap is assumed to be zero, in the new theory it is the energy gap which plays the dominant role. The quasiparticle current creates a population imbalance between the $k > k_F$ and $k < k_F$ branches of the excitation spectrum which relaxes in a characteristic time τ_Q as the current is transferred from the quasiparticles to the pairs.

0 0 0 0 3 9 0 0 7 5 7

II. THEORY

A suitable configuration for isolating the volume of superconductor in which the non-equilibrium processes occur is shown in Fig. 2. A normal metal-insulator-superconductor (NIS) tunnel junction of area w^2 is used to inject electrons into or extract electrons from a volume $\Omega = w^2 d$ of the superconducting strip S'-S-S_p. The dashed lines delineate the tunneling volume labelled S. The pair potential is measured with the superconducting probe S_p and the quasiparticle potential with the normal probe N_p. A difference in potential between the quasiparticles and the pairs V will occur when a current I is flowing. The non-equilibrium volume will be well defined and equal to Ω, and the potential V spatially uniform provided that $w \gg \lambda \gg d$ where λ is the characteristic distance over which V decays.

Tinkham[10] performed a BCS calculation for this potential difference which can be expressed as

$$V = \mathcal{R}(V_{inj}, \Delta, \Omega)\ I \quad , \tag{5}$$

where V_{inj} is the voltage across the injection junction, Δ is the temperature dependent energy gap in S and Ω is the tunneling volume. The quantity $\mathcal{R}$ is the the non-equilibrium voltage per unit current in the superconductor and will be used interchangeably with V/I. We turn now to a detailed discussion of this calculation.

Any system may be described in terms of the occupancy of its quantum states. In a normal metal at equilibrium at a temperature T the probability that a state of wave vector k is occupied is given by the Fermi function $f(k,T) = [\exp(E(k)/k_B T) + 1]^{-1}$ where E(k) is the energy of the state of wave vector k. In a superconductor the state is

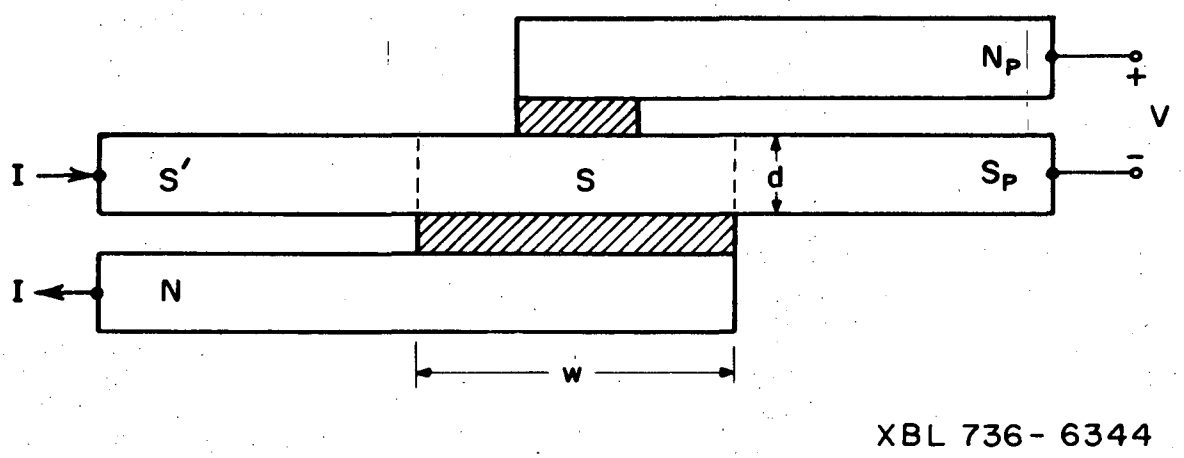

Fig. 2. Configuration for Tinkham's theory for the pair-quasiparticle potential V.

described in terms of the occupancy of pair states $(+\underset{\sim}{k}\uparrow, -\underset{\sim}{k}\downarrow)$. In equilibrium at a temperature T the probability that a pair state is occupied is given by the coherence factor v_k^2 and the probability that the state is unoccupied is given by $u_k^2 = 1 - v_k^2$,

$$v_k^2 = \frac{1}{2}\left(1 - \frac{\varepsilon_k}{E_k}\right) \qquad u_k^2 = \frac{1}{2}\left(1 + \frac{\varepsilon_k}{E_k}\right) , \tag{6}$$

where ε_k is the one electron energy relative to the Fermi energy and $E_k = \left(\varepsilon_k^2 + \Delta^2\right)^{1/2}$. The functions v_k^2 and u_k^2 are shown in Fig. 3 for momenta both greater than and less than the Fermi momentum k_F and are symmetric about k_F to an accuracy of $\sim\Delta/E_F$. The excitation spectrum for a superconductor is also shown in Fig. 3. These excitations are not like the simple electron or hole excitations in a normal metal. The pairing interaction in the superconductor affects the excitation spectrum by introducing an energy gap Δ and by removing the distinction between electrons and holes. An excitation of energy E consists of a mixture of states at momentum $k<$ and $k>$. The state of $k<$ is hole-like $v_{k<}^2$ of the time and electron-like $u_{k<}^2$ of the time. Similarly, the state at $k>$ is electron-like $u_{k>}^2$ of the time and hole-like $v_{k>}^2$ of the time. These follow from the requirement that the excited states be orthogonal to the ground state. To simplify the notation, the wave-vector index in the coherence factors will be dropped (e.g. $v_{k>} \rightarrow v_>$).

Consider now a normal metal-insulator-superconductor (NIS) tunnel junction. An electron from the normal metal entering the superconductor will have a probability $u_<^2$ of entering the $k<$ (hole-like) branch and a probability $u_>^2$ of entering the $k>$ (electron-like) branch. Figure 4(a) shows this process. Conservation of energy requires $E_L + E_R = eV$.

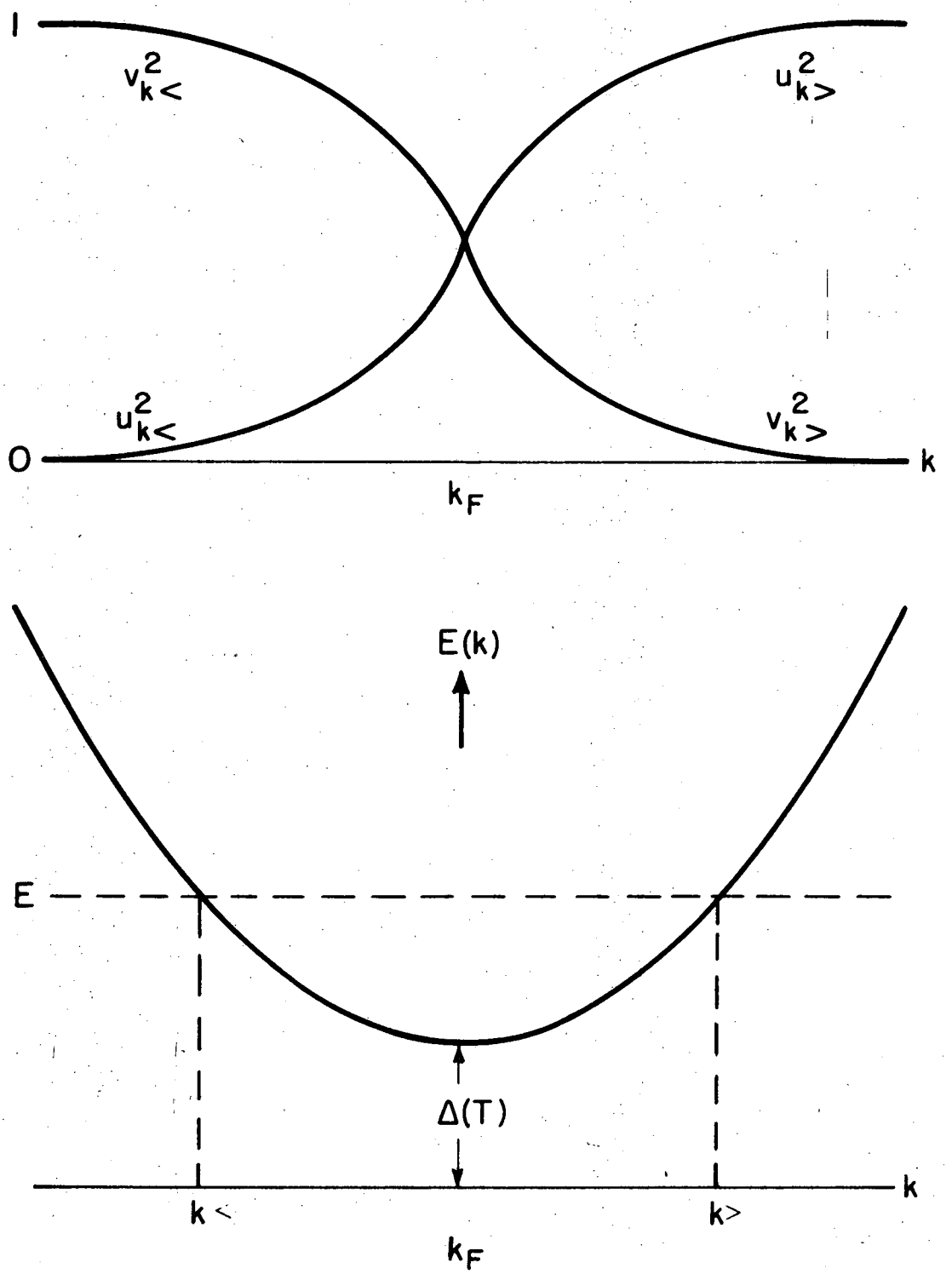

XBL 736-6345

Fig. 3. Coherence factors vs wave vector for a superconductor. Excitation spectrum for superconductor showing degenerate states k> and k< and energy gap Δ(T).

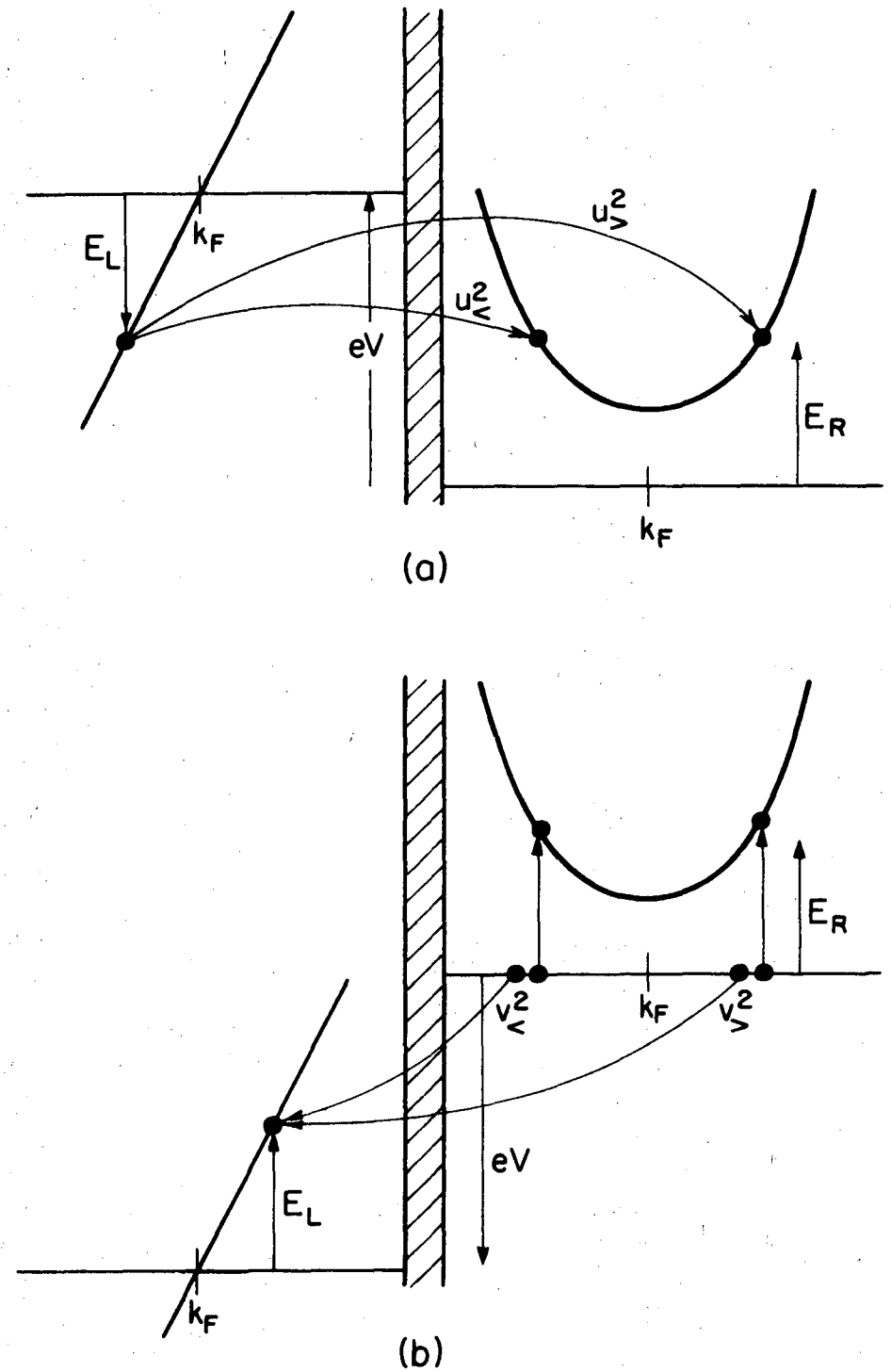

XBL 736-6346

Fig. 4. (a) Schematic diagram for electron injection into a superconductor.
(b) Schematic diagram for electron extraction from a superconductor.

Upon reversing the bias electrons are extracted from the superconductor. This process is shown in Fig. 4(b). A pair is broken and two excitations are created, one in the superconductor and one in the normal metal. The probability that the pair state in question is occupied is v_k^2.

As a result of the difference between $u_>^2$ and $u_<^2$ (for clarity we shall restrict our attention to the case of electron injection into the superconductor) an imbalance in the population of the two branches will be created. The quantity $Q = n_> - n_<$ is the difference in the populations of the two branches per unit volume. A non-zero Q implies that the quasiparticles are carrying current in the superconductor and is closely related to the potential difference V. Q will relax with a characteristic branch crossing time τ_Q in a characteristic distance $\lambda = \tau_Q V_F$ in a clean system ($\ell > \tau_Q V_F$) or $\lambda = (\tau_Q V_F \ell)^{1/2}$ in a dirty system ($\ell < \tau_Q V_F$) where ℓ is the excitation mean free path. The steady state value of Q is just $\dot{Q}_{inj}\tau_Q$ where $\dot{Q}_{inj}$ is the rate at which Q is created by the injection current. Tinkham has shown that $\dot{Q}_{inj}$ is given by

$$\dot{Q}_{inj} = \frac{G_{NN}}{e^2\Omega} \int_\Delta^\infty [f(E - eV_{inj}) - f(E + eV_{inj})]\, dE \quad , \qquad (7)$$

where G_{NN} is the tunneling conductance with the superconductor normal. This quantity differs from the injection current

$$I = \frac{G_{NN}}{e} \int_\Delta^\infty \mathcal{N}(E)[f(E - eV_{inj}) - f(E + eV_{inj})]\, dE \quad , \qquad (8)$$

only by the normalized BCS density of states

$$\mathcal{N}(E) = \frac{E}{(E^2-\Delta^2)^{1/2}} \quad . \qquad (9)$$

The normalized density of states is absent from Eq. (7) because the degree of imbalance $u_>^2 - u_<^2 = u_>^2 - v_>^2 = \mathcal{N}^{-1}(E)$ just cancels the density of states. The degree of imbalance created by the injection current can be expressed by the ratio $\Omega e\dot{Q}/I$ which we define as F,

$$F = \frac{\int_\Delta^\infty [f(E - eV_{inj}) - f(E + eV_{inj})]\, dE}{\int_\Delta^\infty \mathcal{N}(E)[f(E - eV_{inj}) - f(E + eV_{inj})]\, dE} \quad . \quad (10)$$

This function F has been calculated numerically (using dimensionless variables) vs eV_{inj}/Δ for several values of Δ/k_BT and is shown in Fig. 5(a). Figure 5(b) shows this same function F vs $eV_{inj}/\Delta(0)$ for the corresponding values of the reduced temperature t. For $eV_{inj} \gg \Delta$ virtually all of the quasiparticles are created on one branch (the k> branch for electron injection or the k< branch for electron extraction) and $F \approx 1$. For $eV_{inj} \leqslant \Delta$ there are two regimes, $k_BT \gg \Delta$ and $k_BT \ll \Delta$. For $k_BT \gg \Delta$ most of the electrons enter the superconductor at energies high relative to Δ and F remains essentially one. For $k_BT \ll \Delta$ the electrons are injected into states near Δ where $u_>^2 \approx u_<^2$ and F goes to zero. The quantity F has the limiting forms (given by Tinkham)

$$F = \begin{cases} 1 & , \quad T \approx T_c \qquad (11a) \\ 2f(\Delta)/g_{NS} & , \quad eV_{inj} \ll \Delta \qquad (11b) \\ \left(\dfrac{eV_{inj} - \Delta}{eV_{inj} + \Delta}\right)^{1/2} & , \quad T = 0 \qquad (11c) \end{cases}$$

where $g_{NS} = G_{NN}/G_{NS}$ is the normalized conductance of an ideal (NIS) tunnel junction in the appropriate limit. This quantity g_{NS} has been tabulated by Berman[11] for values of eV_{inj} from 0 to 2Δ and for values of Δ/k_BT from 0 to 14.6.

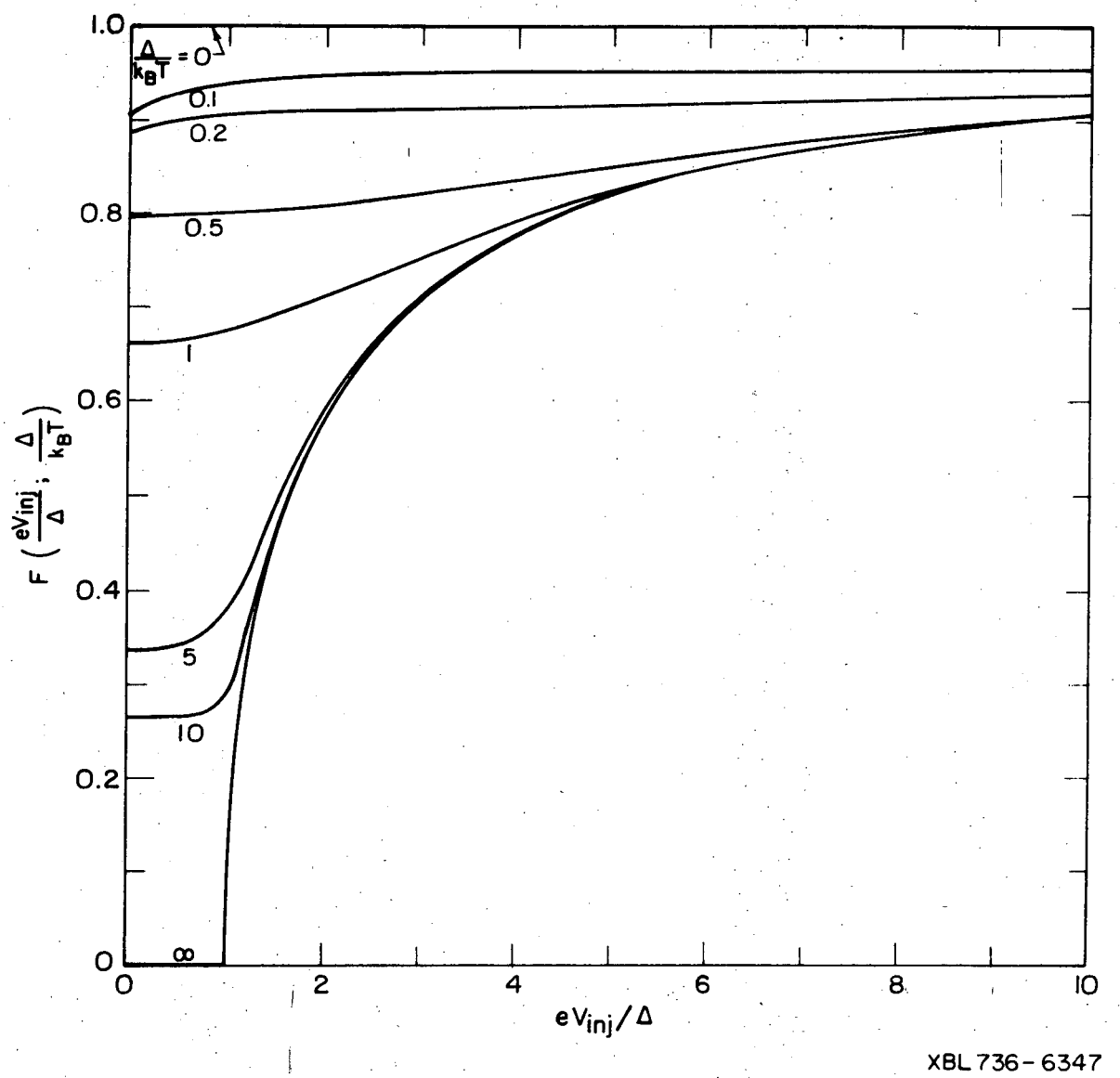

XBL 736-6347

Fig. 5a. Degree of branch imbalance F created by the injection current vs eV_{inj}/Δ for several values of Δ/k_BT.

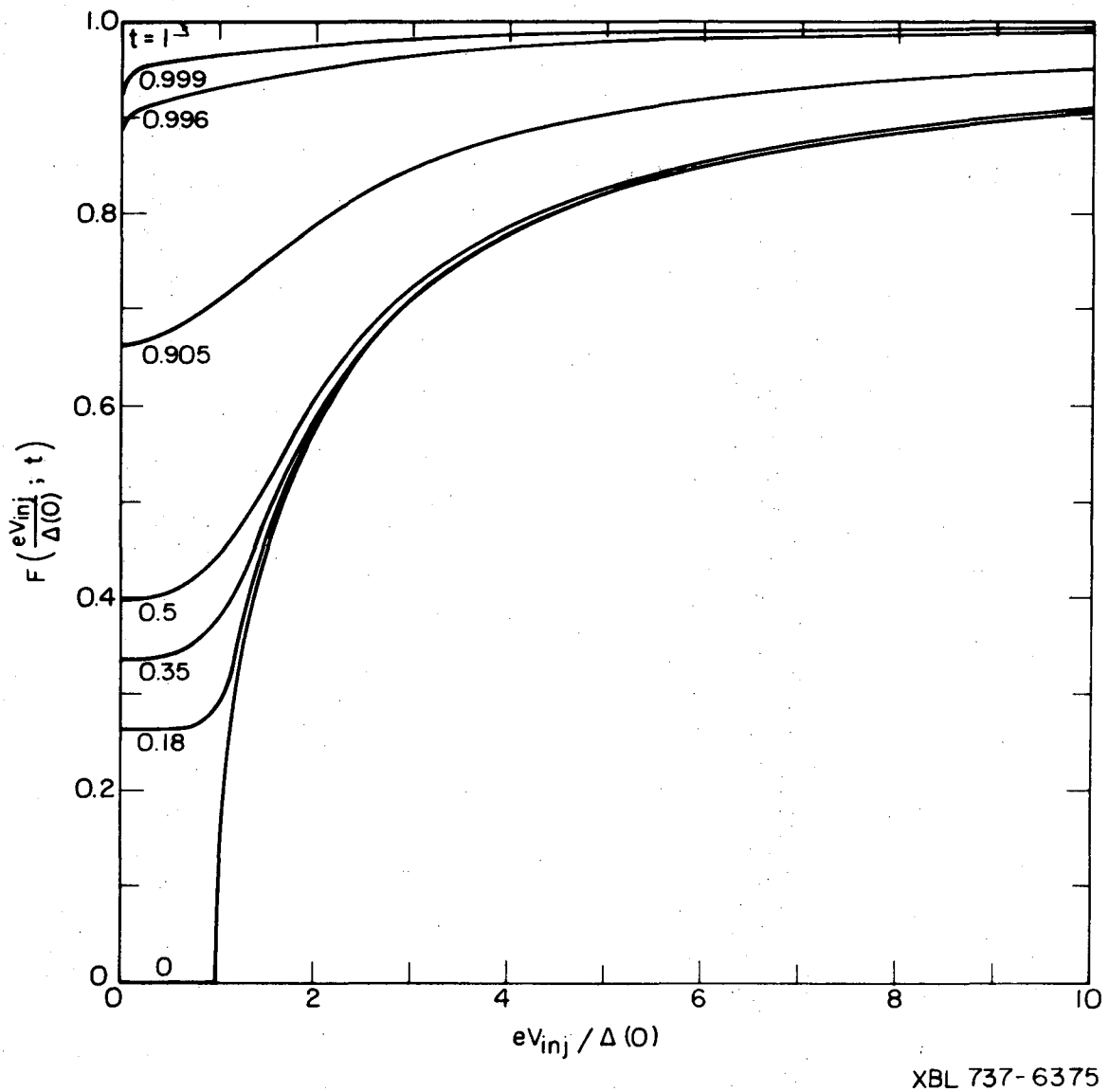

Fig. 5b. Degree of branch imbalance F created by the injection current vs $eV_{inj}/\Delta(0)$ for several values of the reduced temperature.

The population imbalance per unit volume Q is determined jointly by F and τ_Q, $Q = IF\tau_Q/e\Omega$. The pair-quasiparticle potential difference V is related to this imbalance. Consider the system of Fig. 2 with the injection junction carrying a current I; we wish to calculate V. If the normal probe is shorted to the superconducting probe (V = 0) Tinkham has shown that a current

$$I(V = 0) = \frac{G_{NN}}{e} \int_{\Delta}^{\infty} (f_{k<} - f_{k>})\, dE \quad , \tag{12}$$

will flow in the loop. This can be expressed as

$$I(V = 0) = \frac{G_{NN} Q^*}{2N(0)e} \quad , \tag{13}$$

where

$$Q^* \equiv 2N(0) \int_{\Delta}^{\infty} (f_{k>} - f_{k<})\, dE \quad , \tag{14}$$

and N(0) is the density of states per spin in the superconductor at the Fermi level. The quantity Q^* is closely related to Q which is

$$Q = 2N(0) \int_{\Delta}^{\infty} \mathcal{N}(E)(f_{k>} - f_{k<})\, dE \quad . \tag{15}$$

One can now define the non-equilibrium potential V which is the source of this current as

$$V = \frac{I(V = 0)}{G_{NS}} = \frac{Q^*}{2N(0)eg_{NS}} \quad , \tag{16}$$

where $g_{NS} = G_{NS}/G_{NN}$ is the normalized conductance of the normal probe. The normal probe consists of a tunnel junction in series with the normal metal lead. This is the potential which will be measured across $N_p - S_p$ in a null measurement. Near T_c $\Delta \to 0$ and $Q \to Q^*$ but for lower temperatures $Q > Q^*$ and

0 0 0 0 3 9 0 6 7 6 2

$$V_Q \equiv \frac{Q}{2N(0)eg_{NS}} \geqslant V \tag{17}$$

The final results are

$$V = \frac{I}{2e^2N(0)\Omega g_{NS}}\tau_Q \qquad T \simeq T_c \tag{18a}$$

$$V \leqslant \frac{I}{2e^2N(0)\Omega g_{NS}} F\tau_Q \qquad \text{intermediate } \frac{eV_{inj}}{\Delta} \text{ and } T \tag{18b}$$

$$V \leqslant \frac{I\,f(\Delta)}{2e^2N(0)\Omega g_{NS}^2}\tau_Q \qquad eV_{inj} \ll \Delta(T),\ T = 0 \tag{18c}$$

We turn now to a calculation of τ_Q.

The branch imbalance Q can relax by inelastic phonon processes or by elastic processes. The usual scattering probabilities are reduced in a superconductor by terms called coherence factors. In a spatially homogeneous superconductor the coherence factor for scattering of an excitation from a state characterized by (u,v) to one characterized by (u',v') is $(uu' - vv')^2$. The coherence factor for annihilation of two excitations is $(uu' + vv')^2$. The excitation spectrum in a superconductor is very nearly symmetric about k_F. As a result, elastic scattering in an isotropic superconductor ($E = E', \Delta = \Delta'$) is not allowed because $u = v'$ and $v = u'$ and $(uu' - vv')^2 = 0$. The processes which may contribute to branch relaxation are inelastic phonon scattering,

elastic scattering in anisotropic superconductors and elastic seattering due to a spatially varying gap .[12]

The dominant mechanisms near T_c are inelastic phonon scattering and annihilation. The electrons are injected into quasiparticle states from Δ to eV_{inj}. The coherence factors for these inelastic processes are appreciable only when the final state (u',v') lies between Δ and 2Δ; it is therefore sufficient to restrict the final states to this range. (For $E = 2\Delta$, $u_< = v_> \sim 0.03$.) Assuming the initial state on the $k>$ branch has energy $E > 2\Delta$ we have $u \approx 1$, $v \approx 0$ and the scattering and annihilation coherence factors become $(uu')^2$ and $(uv')^2$ respectively. Both of these processes add a pair to the condensate. The relaxation rate will depend on the number of final states between Δ and 2Δ and is therefore proportional to $\Delta(T)$. Tinkham's result for τ_Q near T_c is

$$\tau_Q(T) = 0.068\ \tau_\Theta \left(\frac{\Theta}{T_c}\right)^3 \frac{\Delta(0)}{\Delta(T)}\ ,\ T \simeq T_c\ , \tag{19}$$

where $\tau_\Theta = \ell_\Theta / v_F$ is the scattering time at the Debye temperature. This value is determined by extrapolating from room temperature (see Appendix II). Reducing Θ increases the electron-phonon coupling thereby decreasing τ_Q. The prefactor can be evaluated for tin and lead (see Appendix II) yielding

$$\tau_Q^{Sn}(T) \simeq 2\times10^{-10}\ \frac{\Delta(0)}{\Delta(T)}\ ,\ T \simeq T_c\ , \tag{20a}$$

$$\tau_Q^{Pb}(T) \simeq 3\times10^{-12}\ \frac{\Delta(0)}{\Delta(T)}\ ,\ T \simeq T_c\ , \tag{20b}$$

Tinkham estimates that the values at $T = 0$ will agree reasonably well with the high temperature expression evaluated at $T = 0$.

Elastic scattering can occur for $\Delta \neq \Delta'$. In anisotropic superconductors this will contribute a parallel relaxation channel. Tinkham has obtained an expression for this time

$$\tau_Q^A = \frac{\tau_1}{\langle a^2 \rangle_o} \left[1 + \left(\frac{\hbar}{2\tau_1 \Delta}\right)^2\right]^2 \frac{T^*}{\Delta} \left[1 + \frac{T^*}{\Delta}\right] \tag{19}$$

where τ_1 is the elastic scattering time at low temperatures, T^* is the characteristic temperature of the non-equilibrium distribution of quasiparticles, and $\langle a^2 \rangle_o$ is the mean square bulk anisotropy. The factor $\left[1 + \left(\frac{\hbar}{2\tau_1 \Delta}\right)^2\right]^2$ represents Tinkham's estimate of the reduction in the anisotropy in the films due to Anderson[13] averaging. At T = 0, $\hbar/2\tau_1\Delta = \pi\xi_o/2\ell \sim \pi/2$ for our tin samples ($\ell \sim \xi_o \sim 2000$Å). Assuming $T^* = T_c$ and with $\tau_1 = \ell_1/V_F \sim 3\times10^{-13}$ sec and a bulk mean square anisotropy $\langle a^2 \rangle_o = 0.02$,[14] we obtain $\tau_Q^A(0) \sim 1.5\times10^{-10}$ sec . Near T_c since $\tau_Q^A \sim \Delta^{-6}$ it will be very long. Once ℓ becomes several ξ_o, however, this relaxation process will dominate the inelastic phonon process at low temperatures.

III. EXPERIMENTAL METHODS

A. Sample Preparation for Tin Samples

The samples were prepared on 3 in. × 1 in. glass slides which had been scrubbed with soap and water, rinsed with distilled water and dryed with N_2 gas. Each sample consisted of an Al-oxide-Sn tunnel junction to which had been attached a Cu-Al probe. Each slide contained four such samples; the configuration for one of the samples is shown in Fig. 6. The details for the preparation of each such set of four samples follow.

The Al-oxide-Sn tunnel junctions were prepared by first evaporating a 3 mm wide aluminum strip X - X', 1200Å - 2000Å thick, onto the substrate and then, immediately exposing the film to a one atmosphere mixture of air and nitrogen for a few minutes. The chamber was then evacuated and a 3 mm wide cross strip of tin Y - Y' of the required thickness was deposited. The aluminum was evaporated at pressures of (20-70) × 10^{-6} torr at rates of (20-30)Å/sec. The oxidation mixture varied from 100% nitrogen to 100% air. The tin was evaporated at pressures of (10-50) × 10^{-6} torr at rates of (10-25)Å/sec. This process was repeated until junctions of approximately 0.5Ω were produced. These resistances would increase to 1-2Ω while the sample was being completed; the time for completion and cooling to liquid nitrogen temperatures was typically four hours.

For all but one of the sets of samples the tin was then exposed to air for 20-150 minutes to produce a thin oxide barrier. The slide was then returned to the evaporater and two evaporations of 500Å thick layers of SiO were used to mask off all but an area of 9.4×10^{-3} cm^2

0 0 0 0 3 9 0 3 7 6 3

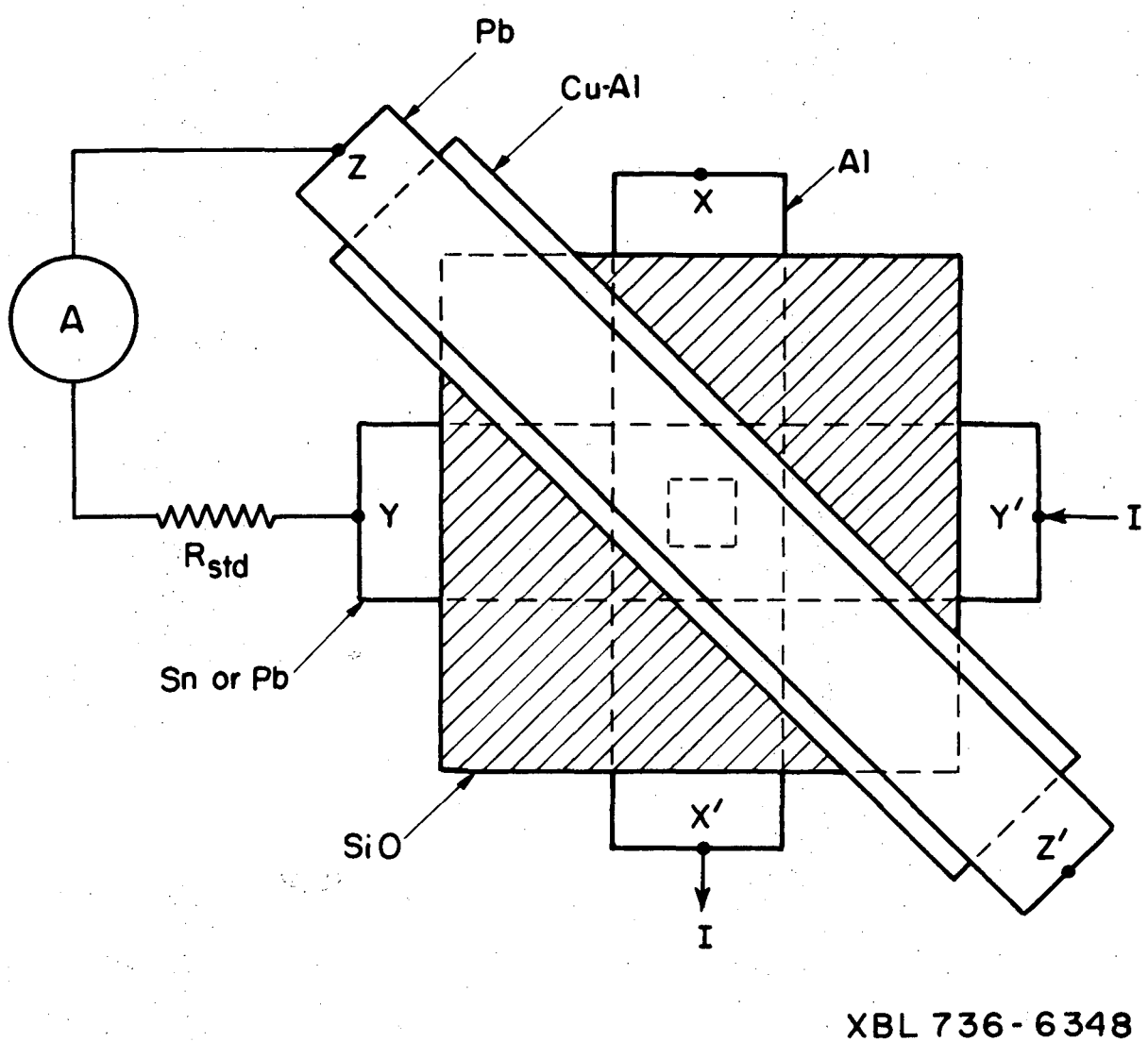

Fig. 6. Experimental configuration for one of the samples showing the standard resistor and the SQUID sensor represented as an ammeter.

in the center of the tunnel junction. A strip of Cu-Al approximately 2μm thick was then deposited diagonally so as to make contact with the tin oxide through the window in the SiO. The Cu-Al served as the normal probe. If the sample had been left like this, the 1 cm length of Cu-Al would have contributed roughly 1Ω to the resistance of the loop in Fig. 6. This would have severely reduced the voltage sensitivity of the circuit for reasons which will be explained in Section III-E. To reduce this resistance, a lead strip Z - Z' was evaporated over the Cu-Al so as to reduce the lead resistance of the strip to $\sim 5\times10^{-7}\Omega$ which is the resistance of the 2 μm thick layer in the window area. The completed normal probe consisted of a superconductor-insulator-normal metal-superconductor junction. The aluminum (3 wt%) was added to the copper to reduce the electron mean free path to ~100Å. This in turn reduced the pair penetration depth in the Cu-Al and precluded pair current flow[15] through the probe. The Cu-Al layer was deposited 1 μm at a time in two separate evaporations. The evaporations were performed with the aid of a pellet dropper which allowed individual pellets, contributing ~200Å each, to be evaporated to completion in succession. The evaporator was opened to air for a few minutes for reloading of the pellet dropper between evaporations; the oxide formed on the copper in that time did not appreciably affect the probe resistance.

The set of samples 11A-11D were made without exposing the tin strip to air. After completion of the tunnel junctions, the SiO and the first 1 μm of the Cu-Al were deposited. The samples were then exposed to air briefly while the lead source was installed and the pellet dropper loaded; the system was then evacuated and the sample

completed. For this set of samples, therefore, the Cu-Al was in good electrical contact with the tin.

B. Sample Preparation for Lead Samples

The configuration for the lead samples was identical to that for the tin samples (see Fig. 6). The preparation of the lead samples followed the same general procedure as that for the tin samples with the following specific differences:

(1) The tunneling barriers were made by oxidizing the aluminum in air for several minutes.

(2) The lead was evaporated at pressures of $(10\text{-}20) \times 10^{-6}$ torr at rates of (30-60)Å/sec.

The Al-oxide-Pb tunnel junctions were found to decrease with time at room temperature. For this reason the desired initial resistances of the junctions were ~2Ω.

C. Shielding

The signal loop consists of the four thin film samples in series with a standard resistor and connecting strips of lead tape. This loop is connected in series with the signal coil within the can containing the SQUID sensor. All extraneous currents flowing in this loop will degrade the S/N of our measurements and must be minimized. The following are the primary noise sources:

(1) vibration of the signal loop in a dc field,

(2) ac flux coupled into the signal loop,

(3) thermoelectric noise due to temperature fluctuations across the standard resistor.

The first two can be minimized by shielding and will be discussed here; the last will be discussed in Section III-E. Figure 7 shows the configuration of the various shields.

Vibrationally induced emf's in the signal loop are minimized by decreasing the magnetic flux, stabilizing this reduced flux and reducing the effective area of the loop. The first is accomplished with the use of concentric mu-metal cans which reduce the earth's dc field to <30 mG and attenuate low frequency magnetic fields to ~100 Hz. The remnant flux within the mu-metal is stabilized by a (superconducting) lead foil cylinder. The effective area of the loop is minimized by taping it (including the glass slide) to a sheet of lead tape which is securely taped to the sample mount. The lead tape provides a superconducting ground plane which decreases the effective area by several orders of magnitude.

External magnetic disturbances are severely attenuated by the

0 0 0 0 3 9 0 3 7 6 5

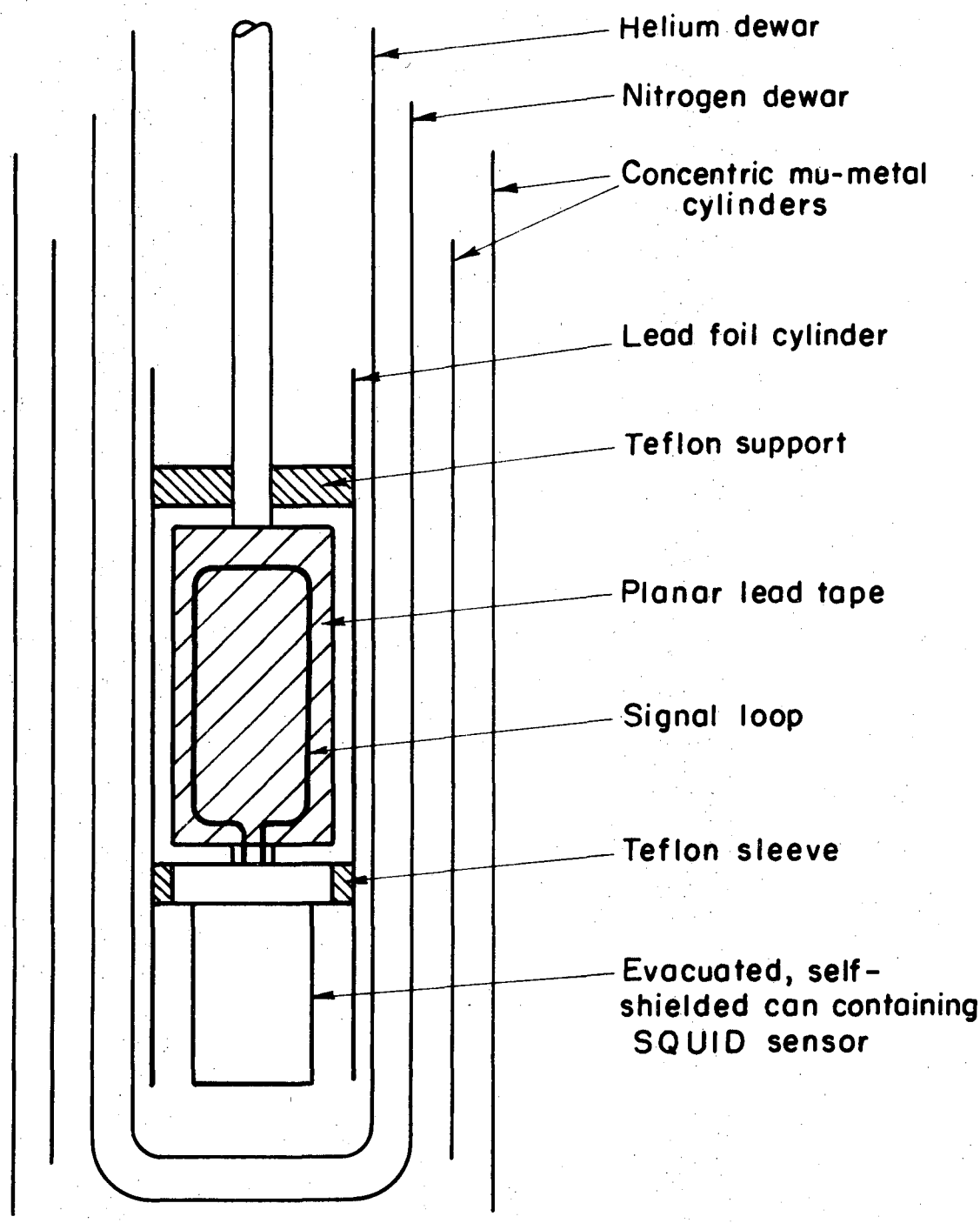

Fig. 7. Configuration of shields for shielding signal loop.

lead cylinder and screened from the signal loop by the ground plane. Further rf shielding was not needed as the experiments were performed in the second basement of a well-shielded building.

D. Electronics

The voltmeter circuit is shown in Fig. 8 and has been discussed in detail by Gifford et al.[16] and by Clarke.[17] It can be divided into three parts: the signal loop, the SQUID sensor and electronics and the feedback circuit.

The signal loop consists of a signal source e_s in series with a source resistance R_S, a standard resistance R_{std} and a total inductance $L_T = L_2 + L_{stray} + L_{std}$ where L_2, L_{stray} and L_{std} are the inductances of the superconducting signal coil, the stray superconducting leads and the standard resistor respectively. The standard resistors used in this work were of two different types. The first consisted of a 1 cm length of 3.5 mm diameter commercial copper wire to which had been attached superconducting leads. This resistor of 0.160 ± 0.004 μΩ served as the primary standard and was calibrated against the current steps on the I-V characteristic[18] of a superconductor-normal-superconductor (SNS)[15] junction irradiated at ~500 kHz. The inductance of this standard is estimated to be $\sim 3\times 10^{-9}$ H. The second standard resistor consisted of a 0.025 cm thick manganin sheet 1 cm square. The superconducting leads were attached to 0.5 cm^2, solder-coated areas on the two faces. This resistor had a resistance of 2.54±0.06 μΩ. The inductance is estimated to be $\sim 10^{-11}$ H.

The SQUID system consisted of a Develco[19] Model 8210 sensor probe, Model 8110 RF Amplifier and a Model 8130 Analog Magnetometer Console.

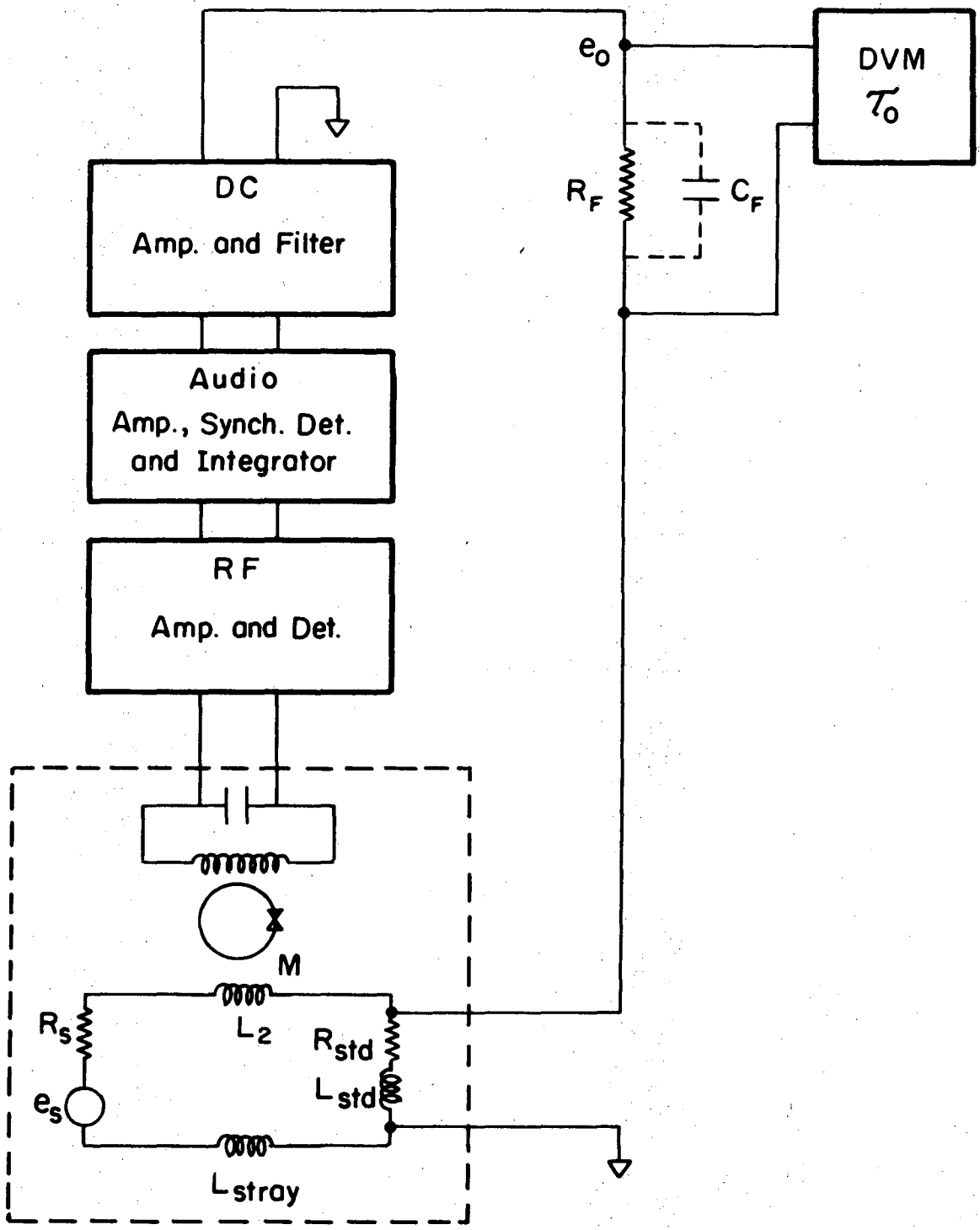

Fig. 8. Closed loop SQUID voltmeter circuit.

The signal loop is coupled to the SQUID sensor via a mutual inductance M. The 30 MHz voltage across the tank circuit is rectified and then synchronously detected at 50 kHz. An integrator with a short time constant smooths the rectified audio; the dc level is amplified and then filtered by an RC circuit (155 seconds). This time constant τ is the dominant one in the loop.

The output e_o provides a feedback current which for $R_F >> R_{std}$ is just e_o/R_F. The feedback capacitor C_F is used to stabilize the loop. The details of the closed loop system including accuracy, stability, bandwidth and input impedance are treated in Appendix I.

E. Noise and Sensitivity

The shielding discussed in Section III-C eliminated noise problems due to microphonics and external fields. Introducing source and standard resistors into the signal loop introduces thermoelectric noise and Johnson noise. For temperatures from 4.2K-2.18K and 2.18K-1.3K the voltmeter was limited by thermoelectric noise and Johnson noise respectively.

Thermoelectric noise is caused by temperature fluctuations along the resistors in the circuit. The voltage noise above the λ point (T_λ = 2.18K) is attributed to thermoelectric noise because of the dramatic decrease in this noise as the temperature was lowered through the λ point and because the thin 2μm Cu-Al barriers in the normal probes did not exhibit this excess noise. The rms voltage noise observed with the copper standard in the circuit was 2×10^{-13} V/$\sqrt{\text{Hz}}$ at 2.5K. The manganin standard was considerably noisier (higher thermopower)

showing an rms voltage noise of 1×10^{-12} V/$\sqrt{\text{Hz}}$ at 2.6K. Assuming a thermopower for the copper at 2.5K of $\sim10^{-6}$ V/K,[20] the observed voltage noise would be expected for rms temperature fluctuations (in a dc to 1 Hz bandwidth) of $\sim2\times10^{-7}$ K/$\sqrt{\text{Hz}}$. Microdegree temperature changes along the 1 cm length of the standard resistor are certainly reasonable. The observed voltage noise above the λ point was typically 10-100 times the expected Johnson noise.

For temperatures below the λ point the voltmeter was limited by Johnson noise in the sample and standard resistors. The Johnson noise voltage is $e_{JN}^{rms} = (4kTRB)^{1/2}$ where R is the total resistance in the signal loop and B is the bandwidth for the measurement.

$$e_{JN}^{rms}/\sqrt{B} = 0.74\ R^{1/2}\ (10^{-12}\text{V}/\sqrt{\text{Hz}}) \text{ at 1K} \quad , \tag{22a}$$

$$= 1.49\ R^{1/2}\ (10^{-12}\text{V}/\sqrt{\text{Hz}}) \text{ at 4K} \quad . \tag{22b}$$

The device noise is expressed as an equivalent noise voltage in the signal loop and is

$$e_{DN}^{rms}/\sqrt{B} = \frac{\varepsilon\Phi_o R}{M} \quad , \tag{23}$$

where ε is the rms device noise expressed as a fraction of a flux quantum Φ_o

$$\varepsilon = \frac{\Phi_{DN}^{rms}}{\Phi_o} \quad , \tag{24}$$

and M is the mutual inductance of the signal coil L_2 and SQUID inductance L. For our SQUID $\varepsilon = 5\times10^{-4}$ /$\sqrt{\text{Hz}}$ and $M = 0.9\times10^{-2}\mu$H yielding

$$e_{DN}^{rms}/\sqrt{B} = 1.1\times10^{-8}\ R\ (\text{V}/\sqrt{\text{Hz}})\ . \tag{25}$$

In Fig. 9 the device noise and Johnson noise are compared over the range of total resistance applicable for this work $(10^{-6}-10^{-4})\Omega$. The SQUID voltmeter is ideal over this temperature and resistance range as the voltage sensitivity is limited by Johnson noise. The noise factor for the device is given by

$$F = \frac{\overline{e_{DN}^2} + \overline{e_{JN}^2}}{\overline{e_{JN}^2}} = \frac{4kTR + \varepsilon^2\Phi_o^2R^2/M^2}{4kTR} \tag{26}$$

One can further define a noise temperature for the device as the temperature at which F = 2. Thus

$$T_N = \frac{\varepsilon^2\Phi_o^2R}{4kM^2} \tag{27a}$$

$$T_N = 240\ R \tag{27b}$$

and even at $R = 10^{-4}\Omega$ the noise temperature is only 24 mK.

F. Measurements

The measurement configuration is shown in Fig. 6. The resistance of the normal probe was measured by passing a current from Z' to Y' and measuring the resulting voltage. I-V plots were recorded on a Hewlett Packard, Moseley Model 7000A X-Y recorder as the current was swept. The nonequilibrium voltage was recorded in an identical manner versus current for both electron injection (current Y' - X') and electron extraction (current X' - Y'). Each slide contained four samples which were wired in series into the signal loop. The experimental data were averaged for those samples (typically two) which had acceptable injection and probe junctions. The film thicknesses were measured using a Varian Å-scope interferometer, Model 980-4000.

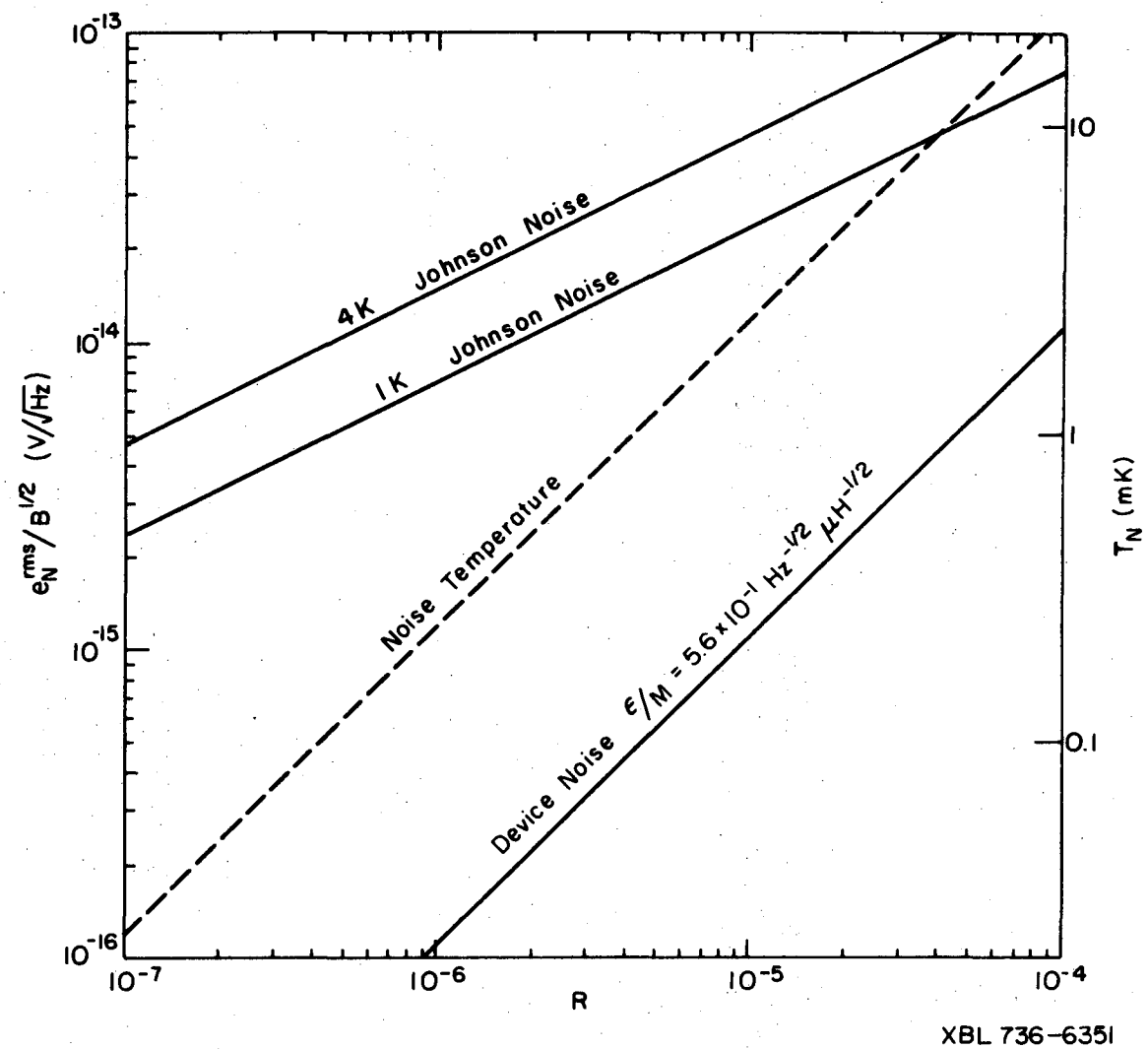

Fig. 9. Johnson noise voltage, device noise voltage and noise temperature vs total signal loop resistance R.

IV. EXPERIMENTAL RESULTS - TIN

Tinkham's theory predicts that the nonequilibrium voltage per unit current $\mathcal{R}$ will be proportional to the product $F\tau_Q$ where F is proportional to the rate at which the branch imbalance is created per unit volume and τ_Q is the relaxation time for this imbalance. Clarke[21] has verified the order of magnitude (10^{-10} sec) and temperature dependence of τ_Q for tin. We present similar results for tin as well as the first experimental tests of the injection voltage and temperature dependences of F. The chapter will be divided into four sections dealing with the injection junction, the probe junction, the determination of τ_Q and the voltage and temperature dependences of F.

A. The Injection Junction

The injection junctions were high quality Al-oxide-Sn tunnel junctions. The resistance of the aluminum strip was $\sim 0.1\Omega$ per square at 4.2K; this allowed us to use junctions of resistance 1Ω and have the tunneling current density uniform to $\sim 10\%$. These low resistance junctions permitted high injection currents and correspondingly high nonequilibrium voltages in the region of special interest, $0 \leqslant e V_{inj} \leqslant \Delta$. The I-V characteristic for the injection junction for sample 6B is shown in Fig. 10 and is representative of the results. The characteristics cover the temperature range (1.37-3.77)K. The aluminum has an energy gap of ~ 0.13 mV at 1.37K. The low voltage portion of this figure was expanded and the slope dI/dV measured as $eV_{inj} \to 0$. The normalized conductance g_{NS} for a BCS superconductor versus Δ/k_BT has been tabulated by Bermon.[11] The value of Δ/k_BT can

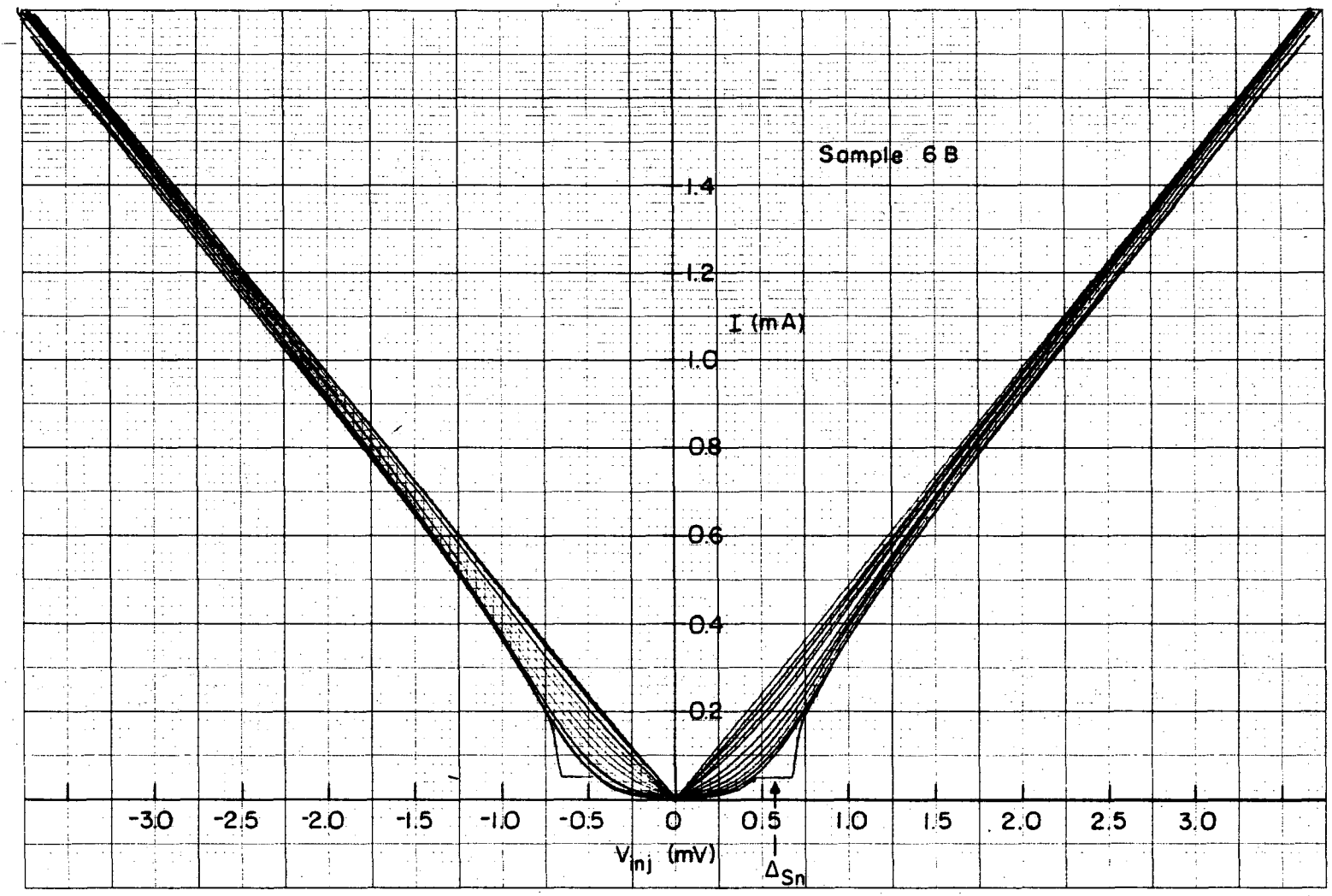

XBL 736-6352

Fig. 10. Injection junction I-V characteristic for sample 6B for temperatures from (1.37-3.77)K.

0 0 0 0 5 6 0 0 7 6 8

be determined from

$$\frac{\Delta}{k_B T} = \frac{\Delta}{\Delta(0)} \frac{\Delta(0)}{k_B T_C} \frac{1}{t} , \tag{28}$$

using the BCS reduced gap and $2\Delta(0) = 3.51\ k_B T_C$[22] for tin. For sample 6C at T = 2.16K the measured and calculated values were both $g_{NS} = 0.245$. The agreement was generally excellent. This process can also be reversed for high quality junctions and the measured values of g_{NS} can be used to determine the energy gap Δ vs T.

B. Probe Junction

The normal probe consisted of a Sn-oxide-Cu/Al tunnel junction in series with the "lead" resistance of the Cu-Al. Both the tunnel junction and the Cu-Al barrier had an area of 8.6×10^{-3} cm^2. The Cu-Al was typically 2 μm thick and was found from measurements on sample 11 to have a resistance of $\sim 5 \times 10^{-7}\Omega$. The resistance of the normal probe at the tin transition temperature was typically $10^{-5}\Omega$ so the Cu-Al contributed at most 5% to the probe resistance.

As the voltage across this tunnel junction was nanovolts or less, the measured normalized conductance must be compared with that for an ideal BCS tunnel junction in the low voltage limit $eV \ll \Delta$. This comparison is made in Fig. 11 for samples 6, 8 and 15. Although sample 6 exhibited considerably more excess conductance than samples 8 and 15, this was not found to affect the values of $\mathcal{R}$.

Also included in Fig. 11 is the conductance of sample 11 for which the tin was not oxidized. For this sample the probe junction consisted of a Sn-Cu/Al-Pb (SNS) junction. The conductance was normalized

0 0 0 0 3 9 0 0 7 6 9

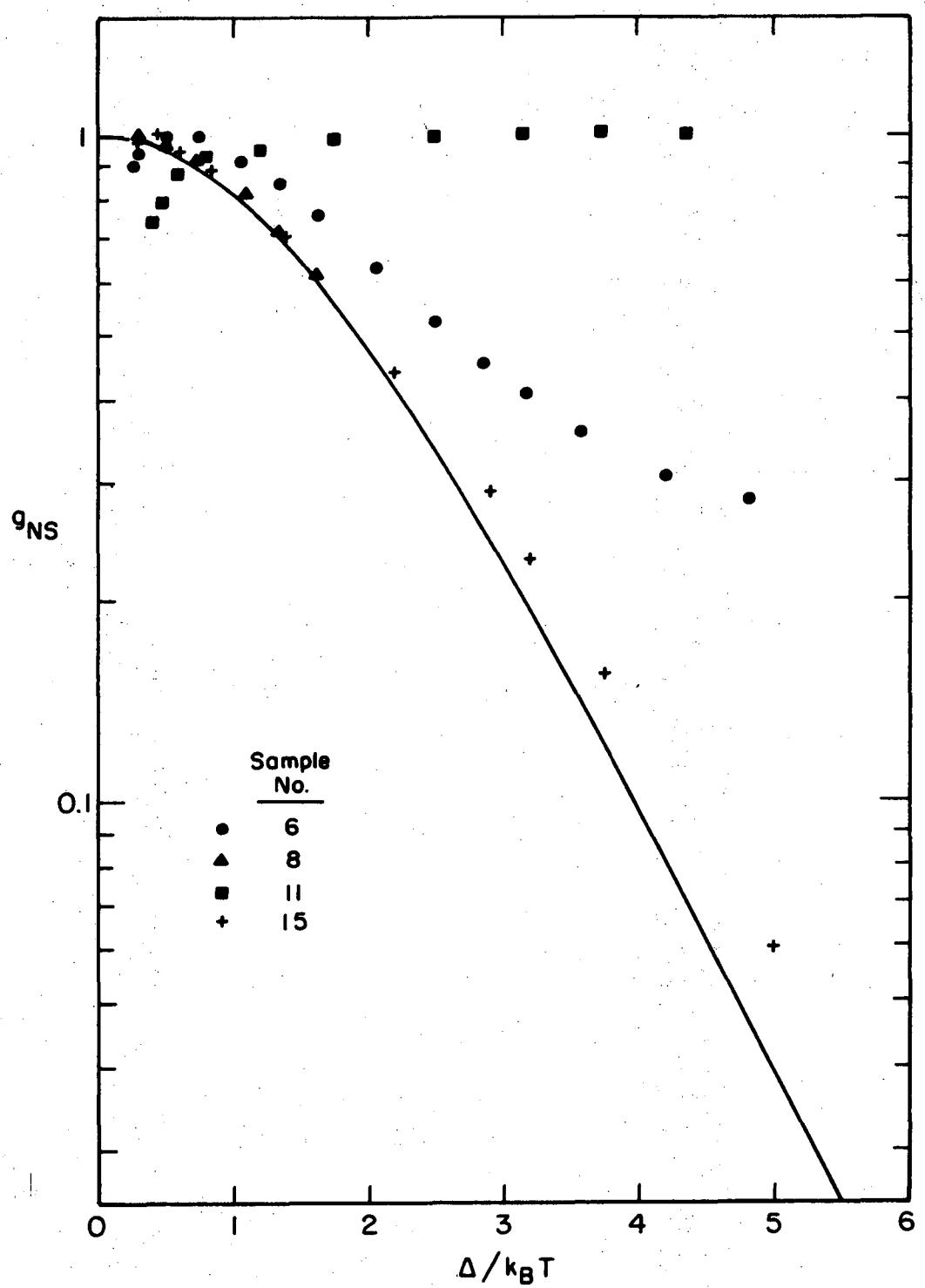

XBL 736-6353

Fig. 11. Normalized low voltage conductance g_{NS} vs Δ/k_BT for the tin samples compared with the theory (solid line) by Bermon.

to the low temperature result. The decrease in the measured conductance near $T_C(\Delta/k_{BT} \to 0)$ reflects the resistive contribution of the tin as a result of the measuring current. This added resistance is just the pair-quasiparticle potential difference per unit current resulting from the measuring current which is applied through leads Y', Z' in Fig. 6. In this case the current is flowing into the superconductor S via an SNS junction but we will soon see that the measured potential is qualitatively the same as for injection via a tunnel junction. Since the measurements of the nonequilibrium voltage V are null measurements (I=0), the normalized conductance used in Eqs. (18) should not include this conductance dip. The oxidized probes exhibited a smaller conductance dip near T_C which was corrected for by normalizing the conductance to the maximum measured value.

C. Determination of τ_Q

For high injection voltages $eV_{inj} \gg \Delta(T)$ Eq. (18) becomes

$$\mathcal{R} \simeq \frac{\tau_Q}{2e^2 N(0) g_{NS} \Omega} , \qquad (29)$$

as F approaches one. We discuss in this section measurements of $\mathcal{R}$ for which $eV_{inj} \geqslant 10\ \Delta(T)$ implying that $F \geqslant 0.9$ (see Fig. 5a).

At each temperature V was plotted continuously versus I for both electron injection and electron extraction. From the X-Y recorder traces the values of $\mathcal{R}$ for $eV_{inj} \approx 10\ \Delta(T)$ were determined. For electron injection into the superconductor the Cu-Al probe was negative relative to S_p; for electron extraction it was positive.

For all samples the values of $\mathcal{R}$ for injection and extraction were nearly equal near T_C but showed a gradually increasing asymmetry as the temperature was lowered. This asymmetry $(\mathcal{R}_{inj}-\mathcal{R}_{ext})/\mathcal{R}_{average}$ at the lowest temperatures was ~ 13% for sample 6 and ~ 50% for sample 15. Since the excitation spectrum is presumed to be symmetric about k_F for $E << E_F$, this result, which was also observed by Clarke,[21] was not expected. The average value $\overline{\mathcal{R}} = \overline{V}/I$ will be used for most of what follows. At low temperatures $\mathcal{R}$ was independent of V_{inj} for $eV_{inj} > 10\ \Delta(T)$ for currents up to the maximum used ~ 20 mA. Near T_C, however, $\mathcal{R}$ increased steadily [even for $eV_{inj} > 10\ \Delta(t)$] and showed increasing instability for injection currents greater than a few milliamperes. This instability is probably a result of temperature fluctuations affecting the energy gap. Reduction of Δ caused by heating attributed to the injection current would also explain the increase in $\mathcal{R}$.

The measured values of $\overline{\mathcal{R}}$ increased rapidly at low temperatures as a result of the rapid decrease of g_{NS}. The data corrected for the measured g_{NS} expressed as $g_{NS}\overline{\mathcal{R}} = g_{NS}\ \frac{\overline{V}}{I}$ are plotted versus temperature in Fig. 12. The quantity $g_{NS}\overline{V}/I$ is seen to be inversely proportional to the volume Ω of the tin for samples 6, 8, and 15. The measured transition temperature for samples 6 and 8 was 3.81K and that for sample 15 was 3.86K. The sample thicknesses are all ± 100 Å and the injection area was constant at 10^{-1} cm^2.

The results for sample 11 show the dramatic effect of the Cu-Al on the energy gap in the tin. The proximity effect reduced the transition temperature to 3.43K and the injection junction I-V characteristic showed no observable energy gap down to the transition

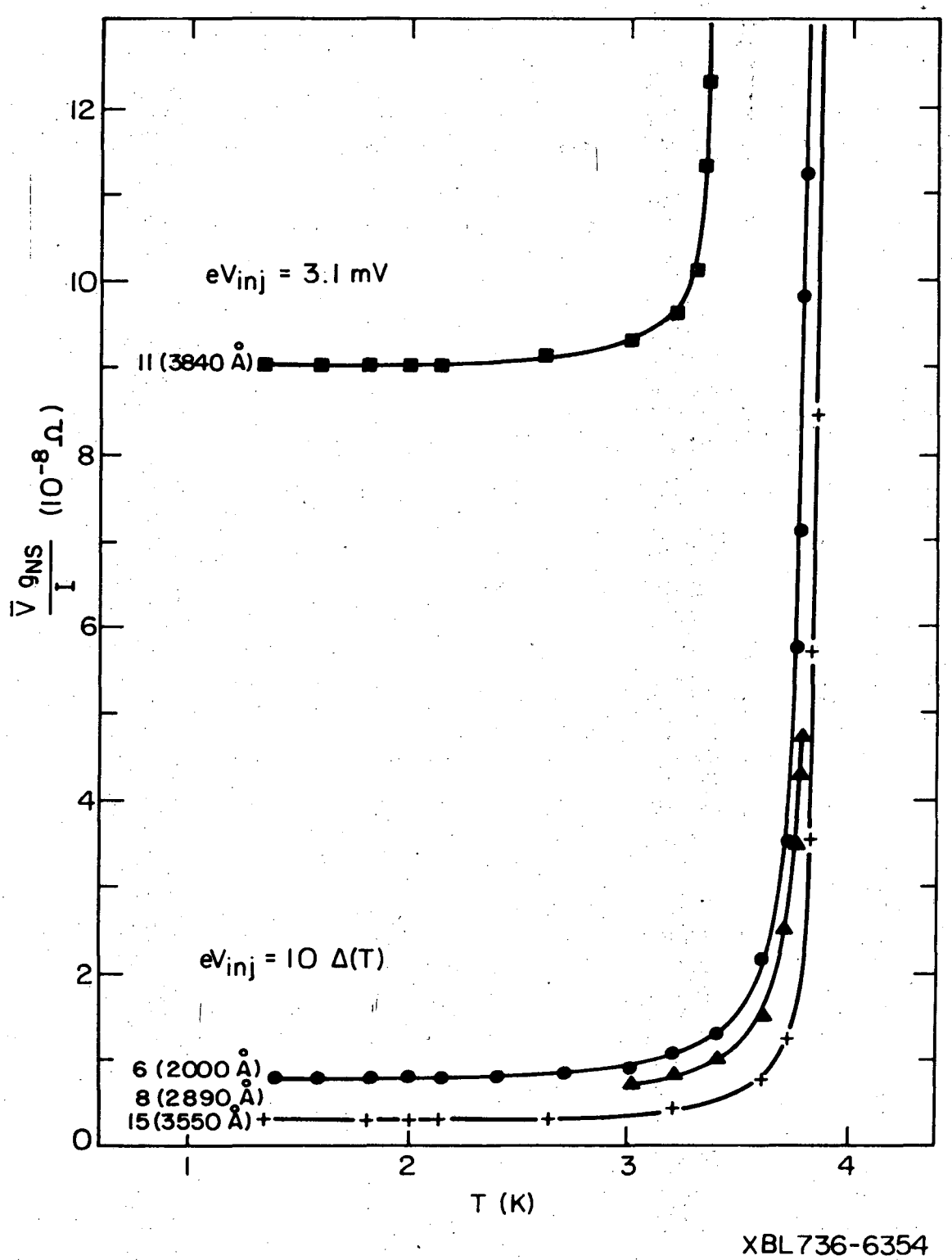

Fig. 12. Average of potential difference per unit current for electron extraction and electron injection corrected for normal probe normalized conductance g_{NS}.

temperature of the aluminum at 1.8K. The small energy gap results in a long τ_Q and a large value of $\bar{V}g_{NS}/I$.

Finally we define a quantity

$$\zeta = \frac{\bar{V}}{I} g_{NS}\Omega = \frac{\tau_Q}{2e^2N(0)}, \qquad eV_{inj} >> \Delta , \qquad (30)$$

which is proportional to τ_Q. This quantity is plotted versus the reduced temperature in Fig. 13(a) where the reduced temperatures T/T_C were determined using the experimentally measured values for T_C. The Tinkham theory predicts a temperature dependence for ζ of $\Delta(0)/\Delta(T)$ near T_C. Figure 13(b) shows the data near T_C with an expanded scale for t. The solid line in Fig. 13(b) represents an attempt to fit the data over the range $0.97 \leq t \leq 1.00$ using only one parameter, the coefficient of $\Delta(0)/\Delta(T)$. The agreement is only fair, indicating that the relaxation of Q near T_C involves more than inelastic electron-phonon processes. The same fit $\zeta = 2.3\ \Delta(0)/\Delta(T)$ is shown as the solid line in Fig. 13(a). At temperatures below about 0.9 T_C, Q^* will be appreciably less than Q and the experimental data are expected to lie below the theory.

Using the value for N(0) for tin from Table I, Appendix II, the fit near T_C implies

$$T_Q = 1.0 \times 10^{-10} \frac{\Delta(0)}{\Delta(T)} \text{ sec} . \qquad (31)$$

The low temperature data imply $\tau_Q(0) = 0.7 \times 10^{-10}$ sec which is in good agreement with Tinkham's low temperature estimate of $Q^*/Q = 0.7$. Clarke[21] fit his data for tin over the entire temperature range to

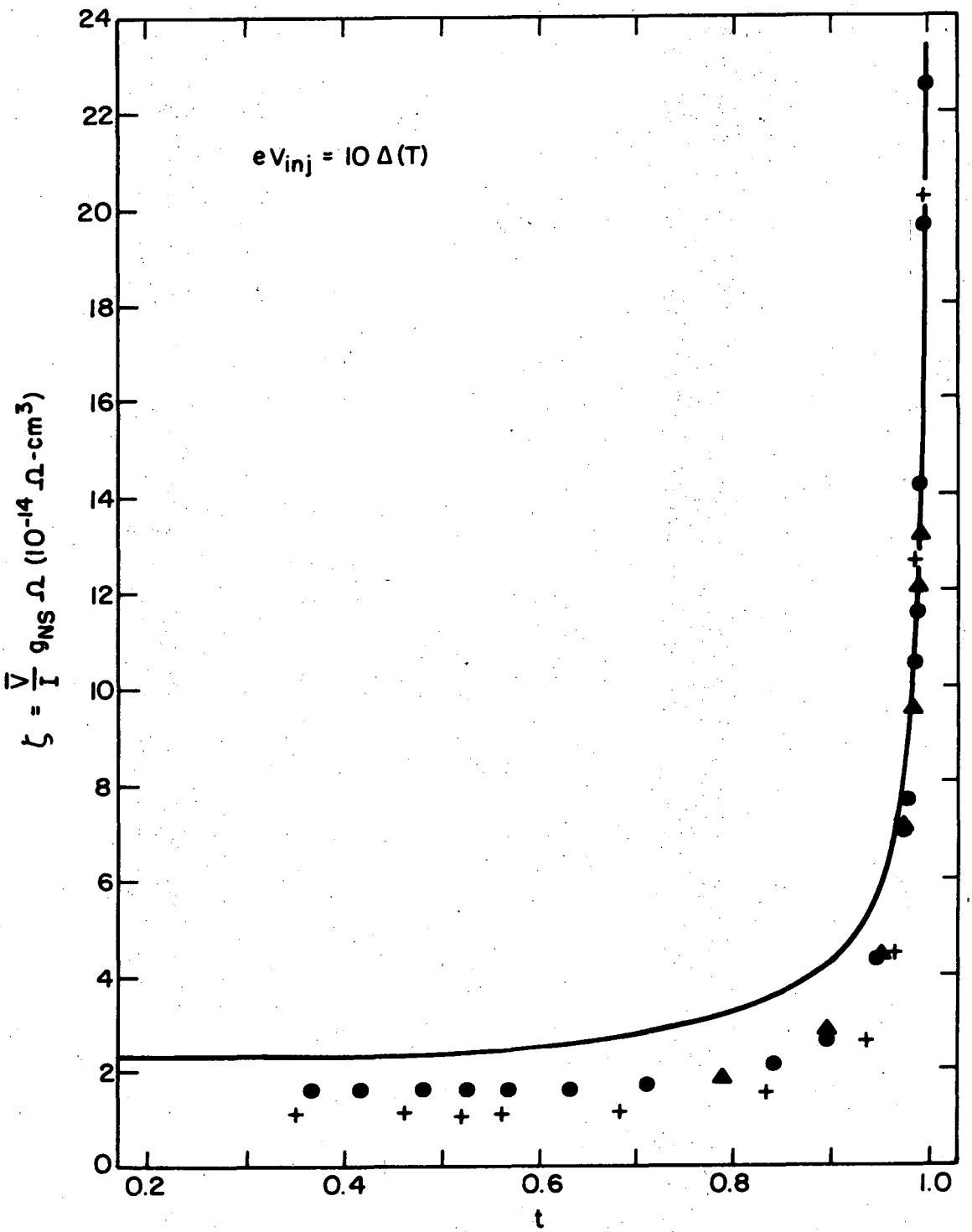

XBL 736-6355

Fig. 13a. The values of ζ for tin samples 6, 8 and 15 vs the reduced temperature. The solid line is the theoretical fit at high temperatures yielding $\zeta = 2.3\ \Delta(0)/\Delta(T)$.

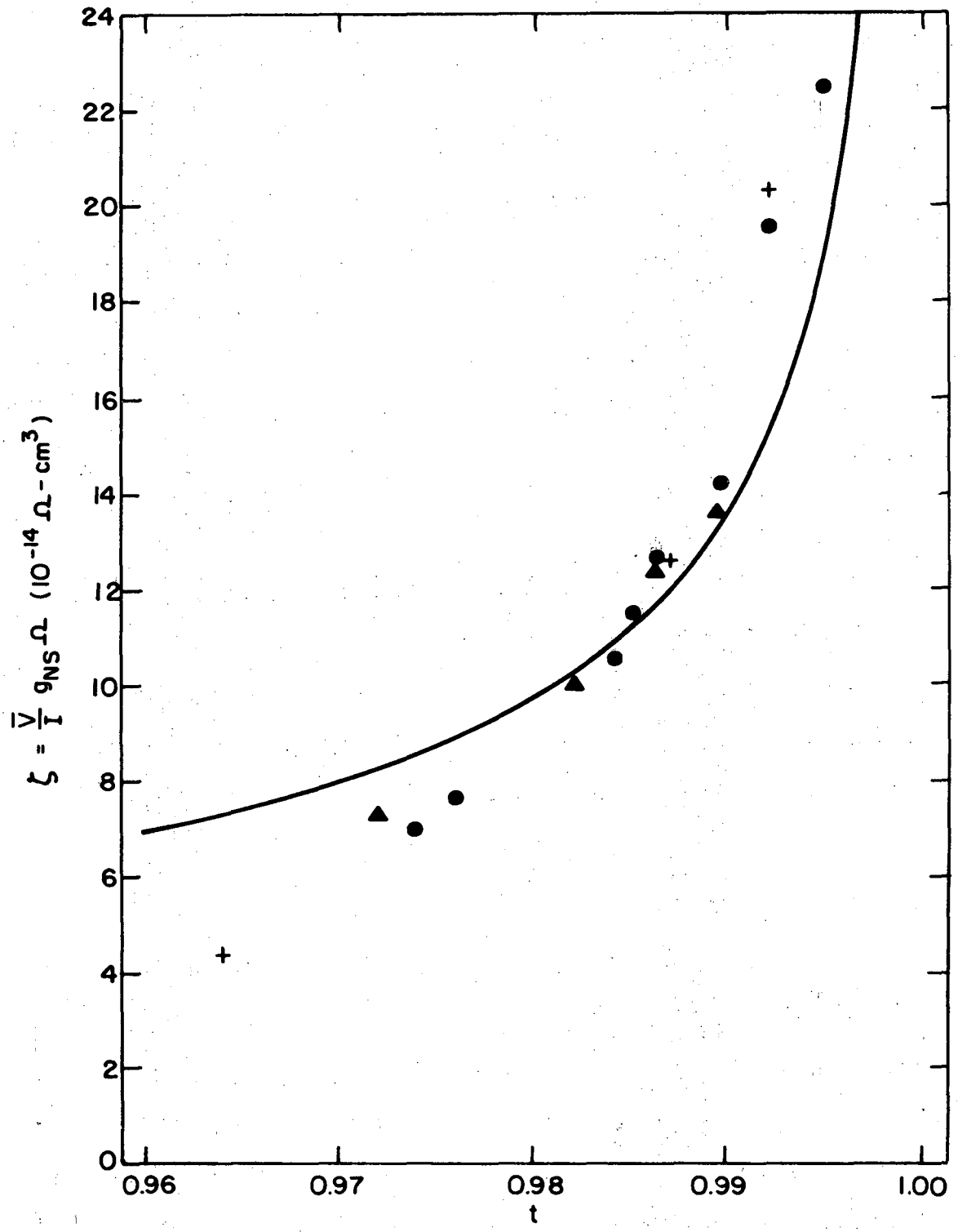

XBL 736-6356

Fig. 13b. The values of ζ for tin samples 6, 8 and 15 vs the reduced temperature t near T_C. The solid line represents an approximate fit to the data of Tinkham's result, yielding $\zeta = 2.3\ \Delta(0)/\Delta(T)$.

obtain $\tau_Q = 3 \times 10^{-10}\ \Delta(0)/\Delta(T)$ sec and $\tau_Q(0) = 3 \times 10^{-10}$ sec. [The published value of 4×10^{-10} was incorrect due to a calibration error.]

Since $V_F\tau_Q$ is at least 46 μm for our samples and $\ell \sim 2600$ Å, the quasiparticles undergo a random walk before branch crossing with a characteristic rms excursion $\lambda = (V_F\tau_Q\ell)^{1/2}$. Near T_C $\tau_Q \sim 10^{-9}$ sec and $\lambda \sim 13$ μm. Since the current-carrying quasiparticles diffuse only ten's of microns along the tin strip, the nonequilibrium volume is well defined by the tunnel junction cross section (3 mm × 3 mm) and the film thickness.

D. The Voltage and Temperature Dependences of F

At high voltages the resistance $\mathcal{R}$ is determined solely by τ_Q. As eV_{inj} is reduced, however, the degree of branch imbalance produced by the injection current is also reduced. The experimental quantity ζ normalized to the limiting value at high voltages ζ_∞ is

$$\zeta/\zeta_\infty = F\left(\frac{eV_{inj}}{\Delta(0)}\ ,\ t\right) \quad . \tag{32}$$

The function F, expressed here in terms of the more obvious experimental quantities $eV_{inj}/\Delta(0)$ and t, is shown in Fig. 5(b). Figure 14 shows a comparison of the experimental values for ζ/ζ_∞ with F for sample 10C at two values of the reduced temperature. The solid lines indicate the experimental results for t = 0.53 and 0.89. The dashed lines indicate the theory for t = 0, 0.5, 0.9 and 1. All of the samples showed a region such as that between 4 and 7 mV in this figure in which ζ exceeded ζ_∞. The reduction in F as eV_{inj} approaches

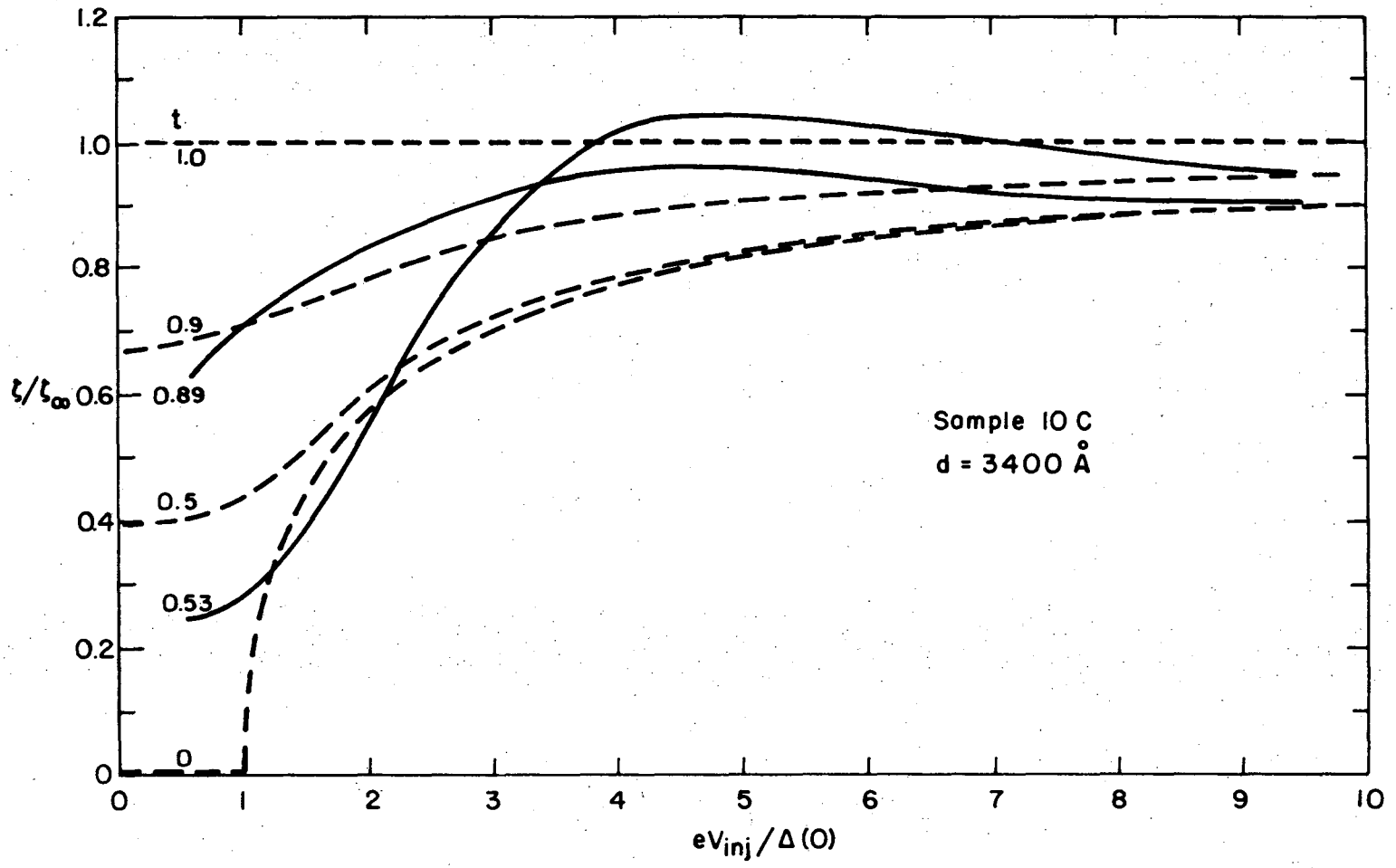

XBL736-6357

Fig. 14. ζ normalized to the high voltage value ζ_∞ vs reduced injection voltage (solid lines) for reduced temperatures 0.53 and 0.89 and F vs reduced injection voltage (dashed lines) for reduced temperatures 0, 0.5, 0.9 and 1.0.

0 0 0 0 3 9 0 0 7 7 2

$\Delta(\Delta = 0.52\ \Delta(0)$ for $t = 0.9$ and $0.96\ \Delta(0)$ for $t = 0.5)$ is clearly seen. Figure 15 shows a similar result for sample 15A. The data at $t = 0.35$ were taken below the transition temperature of the aluminum strip. The general form for F is unchanged as the primary effect of the gap in the aluminum is to simply increase the energy gap in the tunneling density of states to $\Delta_{Al} + \Delta_{Sn}$. The aluminum energy gap at $t = 0.35$ was ~ 0.1 mV.

Figure 16 dramatically shows the effect of V_{inj} on the non-equilibrium potential V. First the I-V characteristic for the injection junction was swept to indicate the discontinuous jump in V_{inj} from approximately $\Delta_{Sn} - \Delta_{Al}$ to $\Delta_{Sn} + \Delta_{Al}$. Electrons are extracted from the tin for $V_{inj} > 0$ and injected into the tin for $V_{inj} < 0$. The non-equilibrium voltage (noisy trace) was then swept and V clearly undergoes a discontinuous change in step with V_{inj}. This clearly demonstrates that the branch imbalance created for $V_{inj} = \Delta_{Sn} + \Delta_{Al}$ is greater than that for $V_{inj} = \Delta_{Sn} - \Delta_{Al}$.

0 0 0 0 9 0 0 0 7 7 3

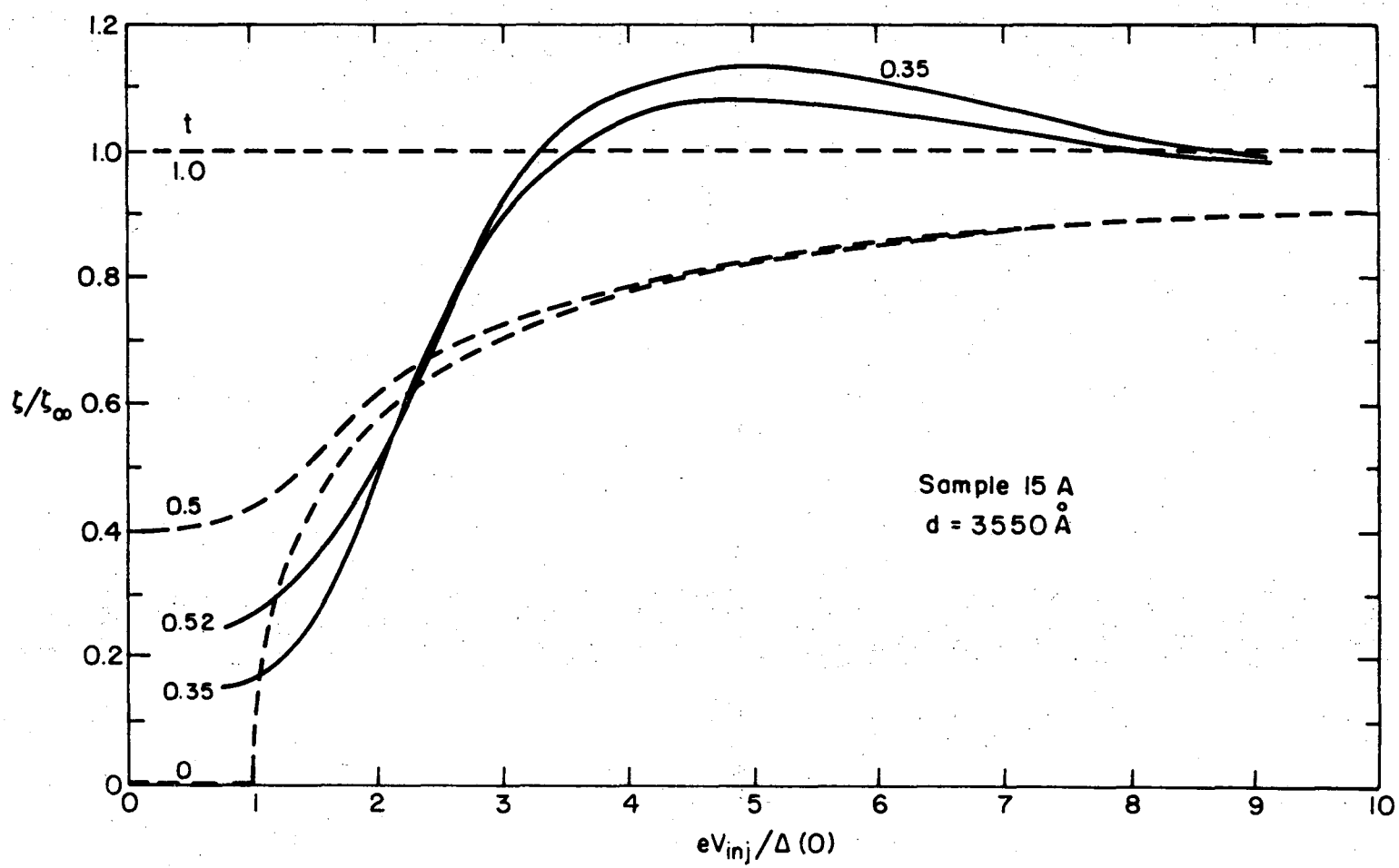

XBL 736-6358

Fig. 15. ζ normalized to the high voltage value ζ_∞ vs reduced injection voltage (solid lines) for sample 15A for two values of the reduced temperature, 0.35 and 0.52. The dashed lines represent the degree of injection imbalance F for values of the reduced temperature of 0, 0.5, 0.9 and 1.0.

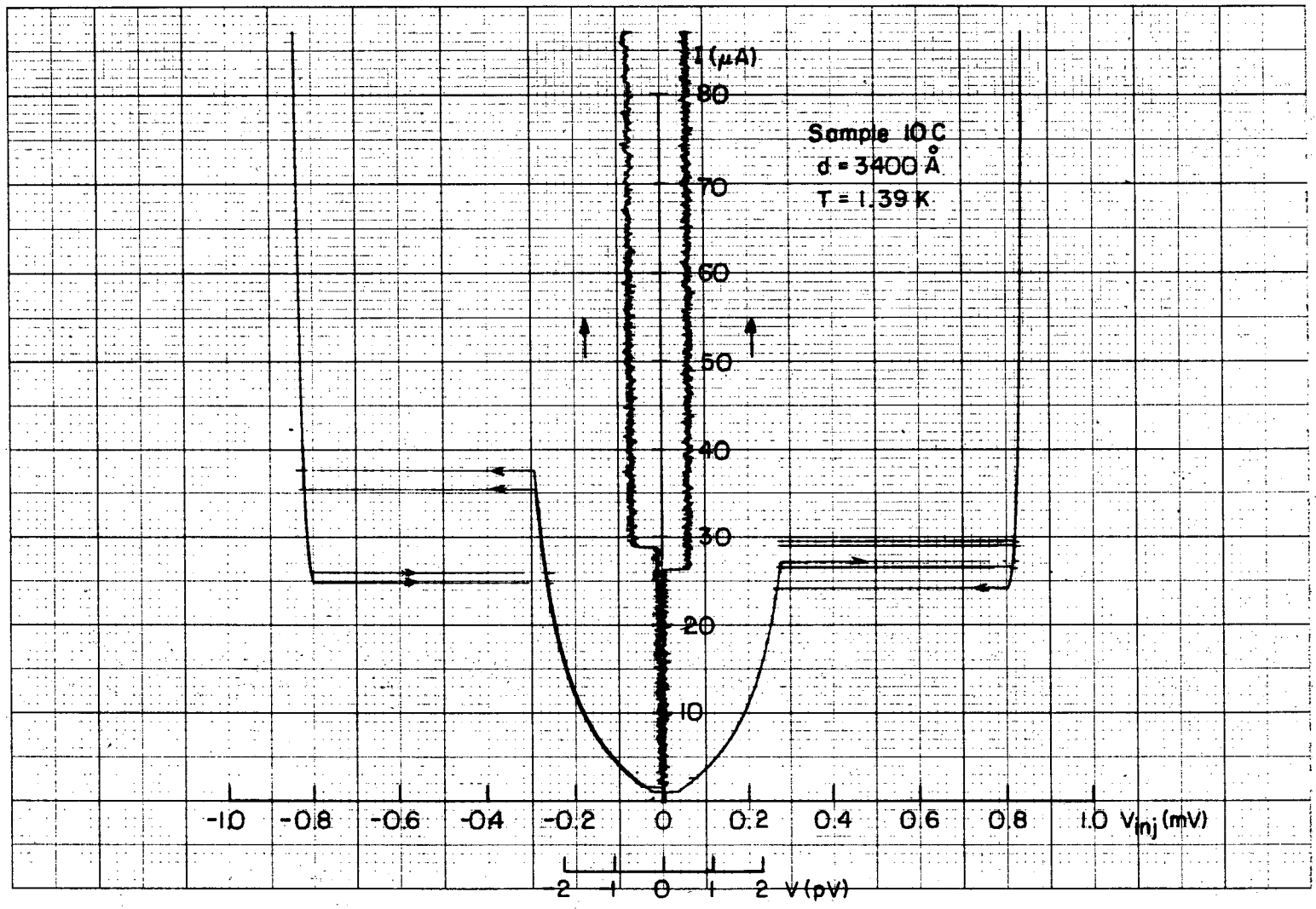

XBL 736 - 6359

Fig. 16. Successive sweeps of the injection voltage V_{inj} and pair-quasiparticle potential difference V vs injection current I for tin sample 10C. Positive and negative voltages represent electron extraction and injection respectively.

V. EXPERIMENTAL RESULTS - LEAD

Measurements were also made on this system with the tin replaced with lead (see Fig. 6) for temperatures from 1.3 to 4.2K. These results will now be discussed.

A. Injection Junction

The Al-oxide-Pb tunnel junction had normal state resistances of 1-2 Ω's. The low voltage portion of one of the tunnel junctions (12 C) is shown in Fig. 17 for temperatures in the range (1.63K-4.22K) over which the aluminum was normal. The limiting resistance for high voltages was 1.5 Ω for this sample. For temperatures above the transition temperature of the aluminum, the low voltage values of g_{NS} can be used to calculate the energy gap Δ. For samples 12C and 12D at T = 2.52K the energy gaps were found to be 1.36 mV and 1.354 mV respectively. Assuming a BCS temperature dependence for the reduced gap, these values yield a value of $\Delta(0) = 1.36$ mV. Tunneling measurements indicate $2\Delta(0) = 4.38\ kT_C$[22] for lead. From this we are able to infer a transition temperature for our films of 7.21K even though no measurements were made above 4.2K. Another requirement for a high quality tunnel junction employing a lead electrode is that the tunneling density of states exhibit the lead phonon structure. For a normal metal-insulator-superconductor junction the derivative of the tunneling I-V curve $(dI/dV)_s$ in the superconducting phase divided by $(dI/dV)_N$ in the normal phase is equal to $\eta(E) = \frac{N(E)}{N(0)}$ where N(E) is the density of quasiparticle states in the superconductor per spin and N(0) is the density of states per spin at the Fermi level in the normal metal. Figure 18 shows an X-Y recorder trace of $(dV/dI)_S$ versus V for junction 12C at 1.63K. The regions of rapidly increasing

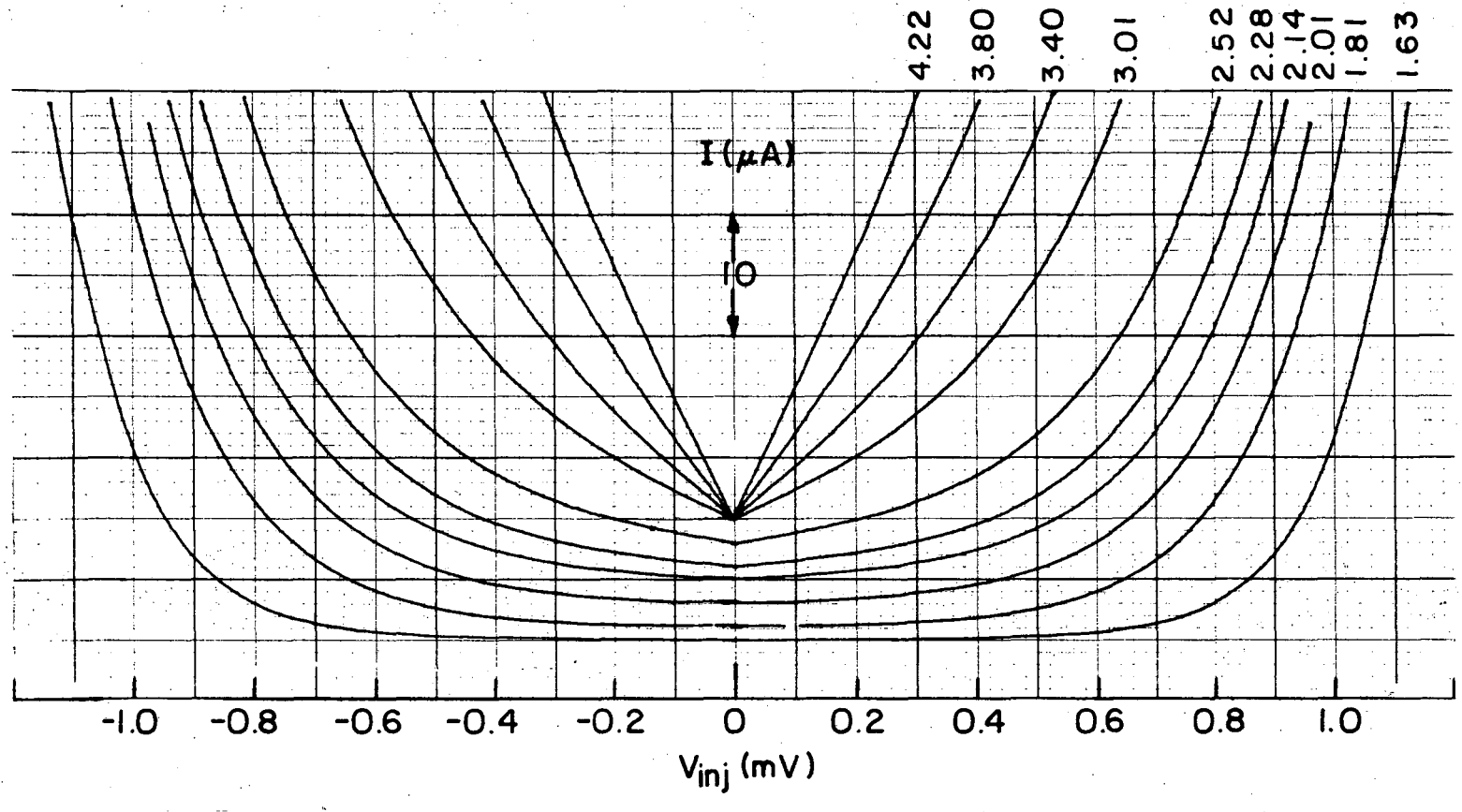

XBL 736-6360

Fig. 17. Low voltage I-V characteristic for sample 12C for temperatures from 1.63K to 4.22K. Successive characteristics are offset for clarity.

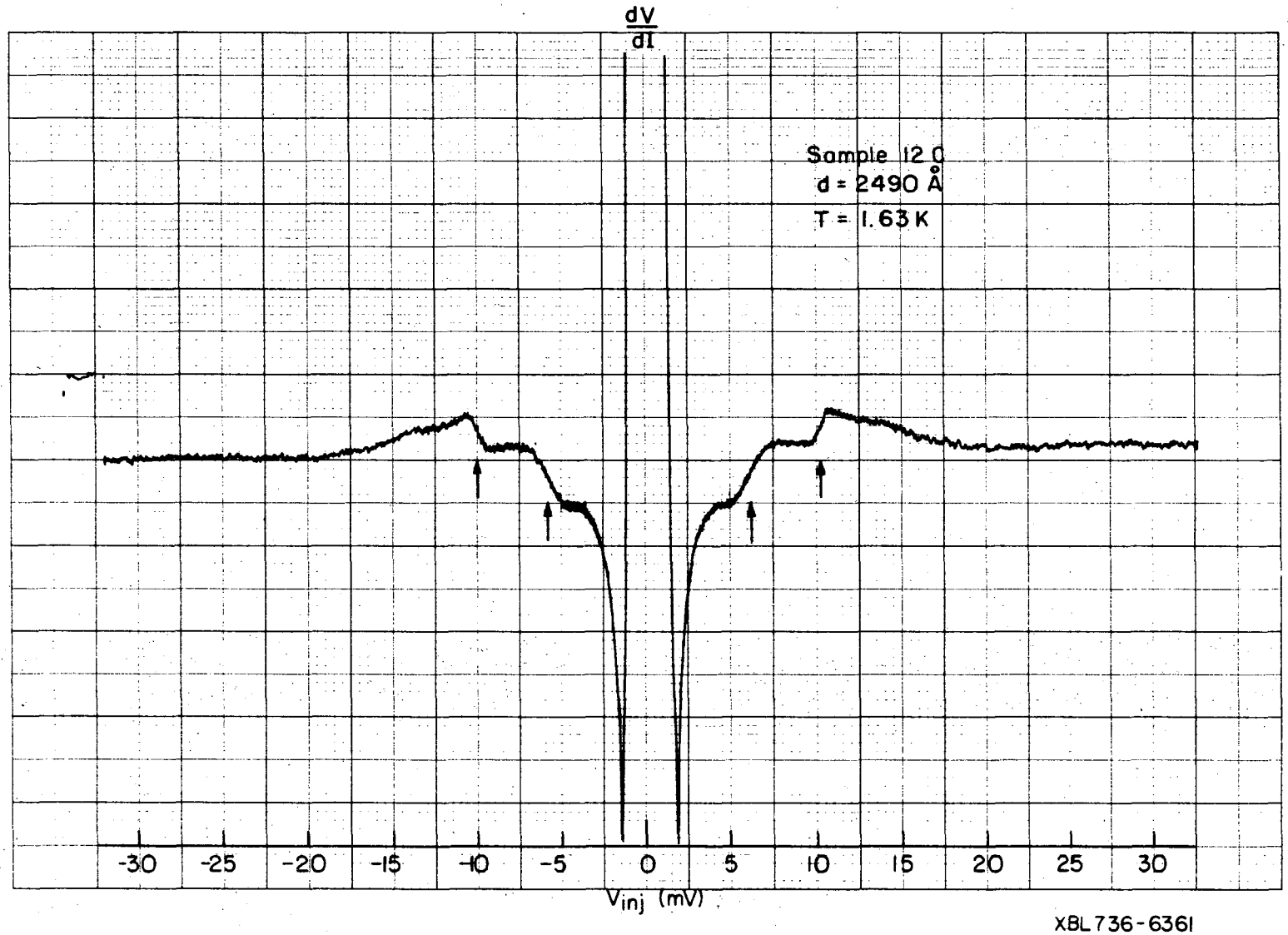

Fig. 18. Dynamic resistance dV_{inj}/dI vs V_{inj} for sample 12C at 1.63K. The arrows indicate the location of the phonon density of states peaks.

0 0 0 0 3 9 0 5 7 7 4

$(dV/dI)_S$ are the result of the phonon density of states peaks for the transverse and longitudinal phonons at energies of 4.5 and 8.4 mV. The peaks occur at voltages of Δ_{Pb} + 4.5 and Δ_{Pb} + 8.4 or ~ 5.9 and 9.8 mV respectively and are indicated by the arrows. The I-V characteristic was swept with a dc current source with an ac modulating current of 35 μA peak to peak.

B. Probe Junction

The Pb-oxide-Cu/Al-Pb junctions had resistances of ~ 5×10^{-6} Ω at 4.2K about an order of magnitude greater than that expected for the Cu-Al barriers alone. The lead films in sample 12 were oxidized in air for 15 minutes and produced probe resistances of 4×10^{-6} Ω at 4.2K; sample 16 was oxidized for 65 minutes and produced probe resistances of 6×10^{-6} Ω at 4.2K. These junctions were not tunnel junctions, however, as the resistances increased only about 5% from 4.2K down to 1.3K. The results for tin, however, indicated that the values of the nonequilibrium voltage were not sensitive to the quality of the probe tunnel junction provided an oxide layer existed. It is likely therefore that the results presented here for lead were not affected significantly by the proximity of the Cu-Al. Additional measurements with better probe tunnel junctions would, of couse, be desirable.

C. Comparison with Theory

The values of the nonequilibrium voltage per unit current for the lead samples showed little asymmetry and were essentially constant for $eV_{inj} > 5\Delta(0)$. The values for electron injection differed from those for electron extraction by only a few percent. The quantity $\zeta = \overline{V}g_{NS}\Omega/I$ was calculated for the two samples and plotted versus the

reduced temperature using the estimated value of $T_C = 7.2K$. The data are shown in Fig. 19 and represent the temperature range 1.3K—4.2K. The data for the two film thicknesses agree very well indicating the expected inverse volume dependence of the nonequilibrium voltage. A solid curve has been drawn through the data points. The data for samples 12 and 16 were taken using a copper standard resistor ($1.6 \times 10^{-7}\Omega$) and a manganin standard resistor ($2.5 \times 10^{-6}\Omega$) respectively. The large error bars for the sample 16 data above the λ point ($t = 0.303$) reflect the order of magnitude more thermoelectric noise across the manganin standard (see Sec. III-E). Tinkham's theory for Q relaxation via inelastic phonon processes predicts a constant value for ζ at low temperatures, $\zeta \simeq \tau_Q(0)/2e^2N(0)$, and Tinkham's estimate is $\tau_Q(0) \simeq 3 \times 10^{-12}$ sec for lead. The value of ζ calculated using this value of $\tau_Q(0)$ and the value of N(0) from Appendix II is $0.5 \times 10^{-15}\Omega\text{-cm}^3$ and is shown as the dashed line in Fig. 19. The value of ζ at 4.2K agrees quite well with the Tinkham estimate for relaxation by inelastic phonon processes. The data, however, imply an increase in τ_Q as the temperature is lowered. This is not expected as additional relaxation channels at low temperatures would cause ζ to decrease.

The low voltage relationship between the injection voltage V_{inj} and the nonequilibrium voltage V is shown in Fig. 20. The X-Y recorder traces were taken at 1.39K, below the transition temperature of the aluminum. No appreciable nonequilibrium voltage is developed for $0 \leq V_{inj} \leq \frac{\Delta_{Pb}-\Delta_{Al}}{e}$ even though an injection current of 150 μA is flowing at $eV_{inj} = \Delta_{Pb} - \Delta_{Al}$. As the I-V characteristic is swept with

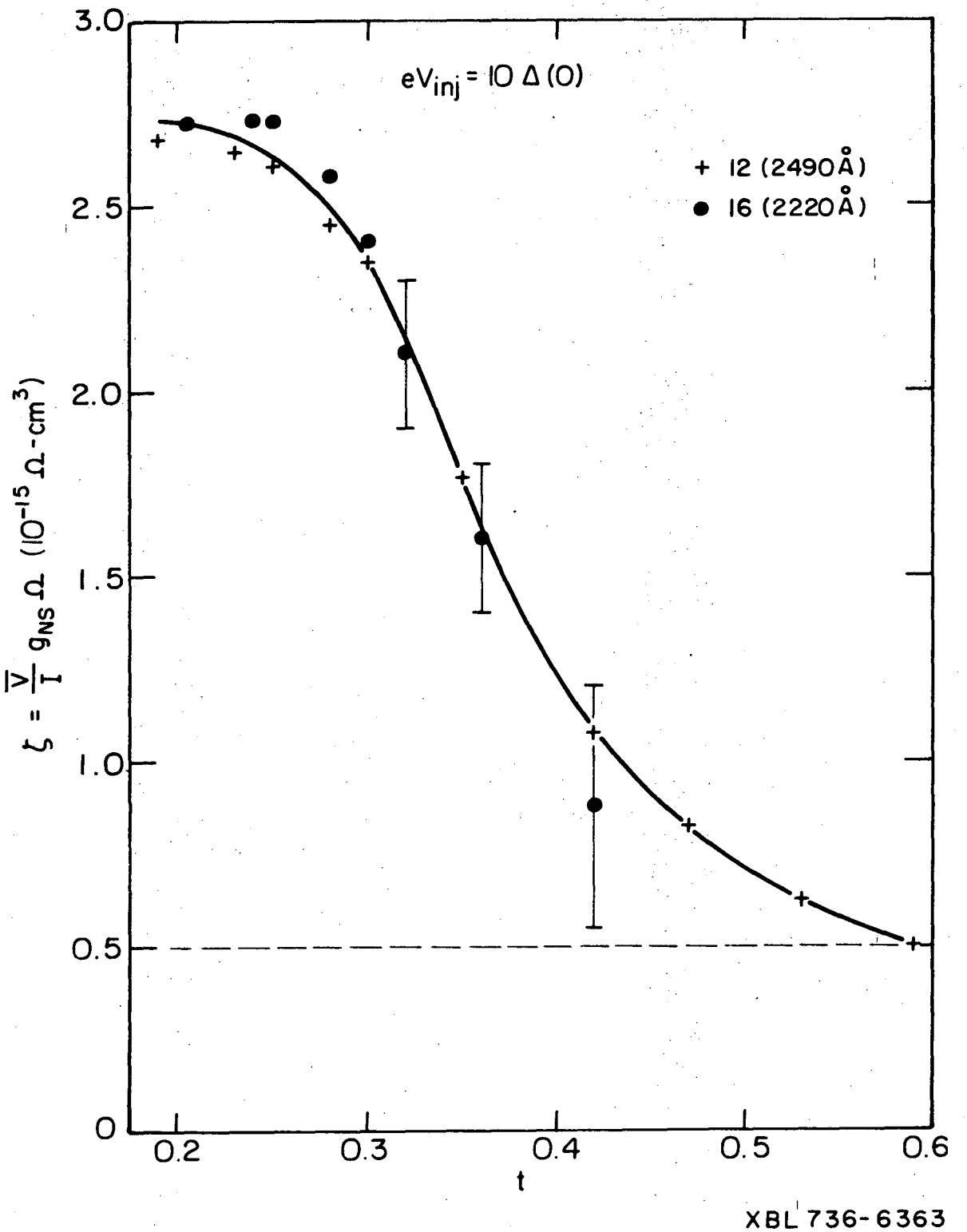

Fig. 19. ζ vs the reduced temperature for lead samples 12 and 16. The solid line is a smooth curve drawn through the data. The dashed line is Tinkham's estimate for ζ.

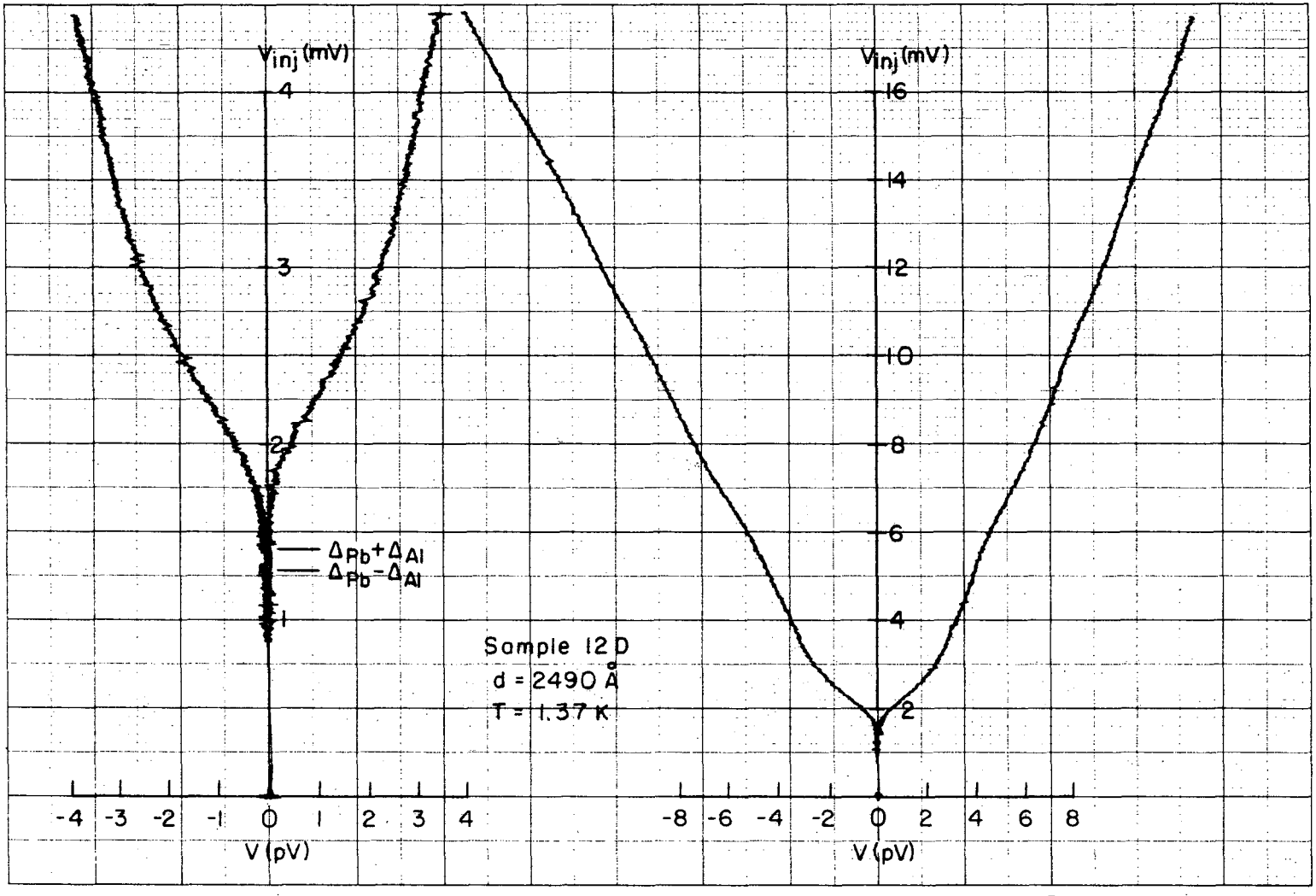

XBL736-6362

Fig. 20. The pair-quasiparticle potential difference V vs the injection voltage V_{inj} for sample 12D at 1.37K. The low voltage portion is enlarged in the trace at the left.

0 0 0 0 3 9 0 0 7 7 6

a current source, the injection voltage jumps discontinuously from $\Delta_{Pb} - \Delta_{Al}$ to $\Delta_{Pb} + \Delta_{Al}$. Above the lead energy gap the nonequilibrium voltage appears and quickly approaches its limiting value with respect to V_{inj}. The ratio of these voltages V/V_{inj} well above the gap approaches $\sim 10^{-9}$ at this temperature.

VI. SUMMARY

We have used an rf SQUID voltmeter to measure the potential difference between the quasiparticles and pairs, in the presence of an electrical current, in a small volume Ω of superconducting tin and lead over the temperature range 1.3K to 4.2K. The current I enters the superconductor through a tunnel junction and produces a branch imbalance in the quasiparticle excitation spectrum. This branch imbalance or quasiparticle current relaxes in a characteristic time τ_Q. The results have been compared with the theory by Tinkham[10] which predicts a nonequilibrium potential V which is proportional to a quantity Q^* which is related to the quasiparticle population imbalance per unit volume Q. Since Q^* cannot be calculated with this simple theory, the theoretical result is expressed in terms of Q. Near T_C, $Q^* \approx Q$ and the theory is expected to agree with the measurements.

Our measurements for tin confirm the volume and injection voltage dependences of V. The temperature dependence of τ_Q is seen to be in fair agreement with the theory near T_C and in excellent agreement at low temperatures. The magnitude of τ_Q near T_C of $1 \times 10^{-10}\ \Delta(0)/\Delta(T)$ sec is in good agreement with the theoretical estimate of $2 \times 10^{-10}\ \Delta(0)/\Delta(T)$ sec and in fair agreement with the results of Clarke[21] of $3 \times 10^{-10}\ \Delta(0)/\Delta(T)$ sec. At low temperatures the data lie below the theory by an amount which is consistent with Tinkham's estimate of $Q^*/Q \sim 0.7$. One sample utilized a normal probe which was in good electrical contact with the tin. The tin electrode exhibited no observable energy gap and V remained large at low temperatures, as expected, since V is proportional to $\Delta(0)/\Delta(T)$.

Our measurements for lead confirm the volume and injection voltage dependence of V. The data near 4.2K agree with Tinkham's low temperature estimate of $\tau_Q \simeq 3 \times 10^{-12}$ sec. Below 4.2K, however, V increases; this was not expected and is not understood at the present time.

ACKNOWLEDGMENTS

I would like to thank my advisor John Clarke for suggesting this research project and for his interest and advice throughout this work. I would also like to thank Richard Voss for the computer calculations of F used in Figs. 5a, 5b, 14 and 15. Finally, I wish to express my thanks to my wife Carol for her continued encouragement and support throughout my tenure at Berkeley.

This work was done under the auspices of the U. S. Atomic Energy Commission.

APPENDIX I. FEEDBACK ANALYSIS

The voltmeter circuit shown in Fig. 8 will be discussed in detail here with a treatment which closely follows that by Gifford et al.[16] The circuit can be formally analyzed using the block diagram shown in Fig. 21. The summing point is the SQUID sensor; the net flux $\Delta\Phi$ in the sensor is given by $\Phi_S - \Phi_F$ where Φ_S is the signal flux and Φ_F is the feedback flux. The forward, flux-voltage transfer function G is

$$G(\omega) = \frac{G(0)}{1 + j\omega\tau} \quad ; \; \tau = RC \quad , \tag{1}$$

where τ is the dominant time constant (~100 secs) in the circuit. The signal and feedback transfer functions are easily calculated by referring to Fig. 8.

$$g_s = \frac{M}{(R_s + R_{std})(1 + j\omega\tau_s)} \quad ; \quad \tau_s = \frac{L_2 + L_{stray} + L_{std}}{R_s + R_{std}} \quad , \tag{2}$$

$$g_F = \frac{M\, R_{std}}{R_F(R_s + R_{std})} \; \frac{(1 + j\omega\tau_F)(1 + j\omega\tau_{std})}{(1 + j\omega\tau_s)}$$

where $\tau_{std} = L_{std}/R_{std}$ and $\tau_F = R_F C_F$. The voltage gain e_o/e_s can be calculated with the help of one additional equation,

$$\Delta\Phi = \Phi_S - \Phi_F \; . \tag{4}$$

The open loop gain A_{OL} ($\Phi_F = 0$) is

$$A_{OL} = g_s G = \frac{G(0)\, M}{(R_s + R_{std})} \; \frac{1}{(1 + j\omega\tau_s)(1 + j\omega\tau)} \quad . \tag{5}$$

The closed loop gain A_{CL} is

$$A_{CL} = \frac{g_s G}{1 + g_F G} = \frac{A_{OL}}{1 + G_L} \quad , \tag{6}$$

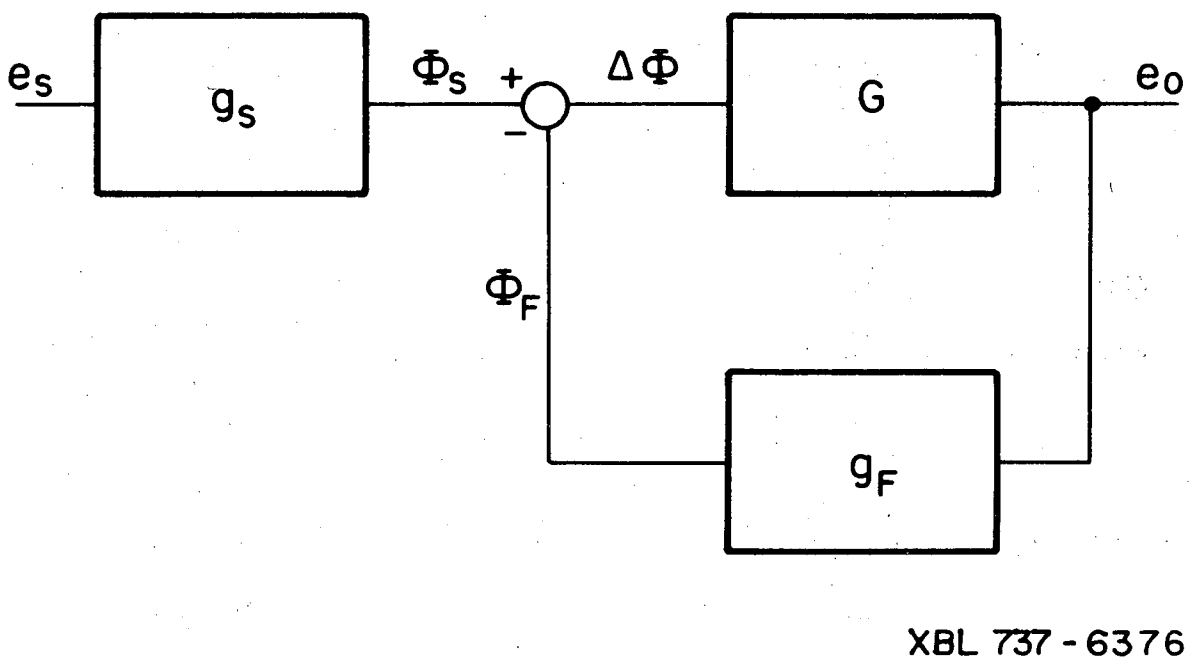

Fig. 21. Block diagram for SQUID voltmeter.

where $G_L = g_F G$ is the loop gain. Using these definitions, we consider stability, bandwidth, accuracy and input impedance for the closed loop system.

A. Loop Gain and Stability

The general expression for the loop gain is

$$G_L = \frac{G(0)\ M\ R_{std}}{R_F(R_s + R_{std})} \frac{(1 + j\omega\tau_F)(1 + j\omega\tau_{std})}{(1 + j\omega\tau_s)(1 + j\omega\tau)} , \tag{8}$$

$$G_L(0) = \frac{G(0)\ M\ R_{std}}{R_F(R_s + R_{std})} \tag{9}$$

The stability of the system requires that for $G_L > 1$ the feedback be negative. The feedback will remain negative so long as the phase of the complex loop gain function is less than $\pi/2$. For the usual case ($\tau > \tau_s > \tau_{std}$) this requirement will be met independent of the frequency provided $\tau_F \geqslant \tau_s$, i.e.,

$$R_F C_F \geqslant \frac{L_2 + L_{stray} + L_{std}}{R_{std} + R_s} . \tag{10}$$

If the feedback capacitor is not used, the phase will reach $\pi/2$ at an angular frequency $(\tau\tau_s)^{-1/2}$ and the maximum allowable loop gain will be $(\tau/\tau_s)^{1/2}$.

B. Bandwidth

The bandwidth for the closed loop system $(2\pi\tau_{FB})^{-1}$ greatly exceeds that for the open loop system $(2\pi\tau)^{-1}$. We calculate τ_{FB} for the case $\tau_F = \tau_s$. Using Eqs. (1), (2), (3), (6) and (9) the closed loop voltage gain becomes

$$A_{CL} = \frac{g_s(0)\ G(0)}{(1 + j\omega\tau) + G_L(0)\ (1 + j\omega\tau_{std})} \quad ,$$

$$= \frac{A_{OL}}{1 + j\omega(\tau_{std} + \tau/G_L(0)} \quad . \tag{11}$$

The voltage gain begins rolling off at 3dB/octave at a frequency B_{FB},[24]

$$B_{FB} = (2\pi\tau_{FB})^{-1} = \frac{R_{std}}{2\pi L_{std}} + \frac{\tau}{2\pi G_L(0)} \quad . \tag{12}$$

C. Accuracy

The fractional error in the output e_o as a result of the error signal can easily be shown to be

$$\frac{\Delta\Phi}{\Phi_s} = \frac{1}{1 + G_L} \quad . \tag{13}$$

For dc measurements with $G_L(0) >> 1$ the accuracy is $100/G_L(0)\%$. For periodic inputs at an angular frequency ω the accuracy is reduced to $100/G_L(\omega)\%$.

Often the input consists of a voltage ramp. For the case in which the closed loop voltage gain can be written as in Eq. (11) with a single term $(1 + j\omega\tau_{FB})$ in the denominator, the system responds to ramp inputs in the same way as a simple RC filter circuit. Suppose the input is swept to a voltage e_{smax} in a time T. It is easy to show that for times $T >> \tau_{FB}$ the output e_o will be delayed with respect to the input e_s by a time τ_{FB} and the resulting output voltage error at time T will be $e_{omax}\ \tau_{FB}/T$ where e_{omax} is the output which would result from a dc input e_{smax}. The percentage error in e_o will be $100\ \tau_{FB}/T\%$. If the sweep stops at e_{smax}, the output voltage will approach the value e_{omax}, the value characteristic of the dc accuracy of the measurement, in a time characterized by τ_{FB}.

D. Input Impedance

Gifford et al.[16] have shown that for the case $\tau_F = \tau_s << \tau$ the input impedance Z_{in} for the system is

$$Z_{in} \approx R_{std}\, G_L(0) \frac{1}{(1 + \omega^2\tau^2)} + j\left[\omega L_T - R_{std}\, G_L(0) \frac{\omega\tau}{1 + \omega^2\tau^2}\right] \qquad (15)$$

The input impedance is real and enhanced by the loop gain at dc.

E. Estimate of Accuracy

The feedback capacitor C_F was not used for our measurements. The resulting loop gain was in the range $4\times10^3 < G_L(0) < 10^4$. The major time constant τ was 155 seconds and τ_{std} was estimated to be $\sim2\times10^{-2}$ sec for the $1.6\times10^{-7}\Omega$ standard which was used for most of the measurements. The feedback time constant τ_{FB} calculated from Eq. (12) is, therefore, $\tau_{FB} < 6\times10^{-2}$ sec. The input was swept at rates $<10^{-12}$ V/sec implying an absolute accuracy of better than 6×10^{-14} V.

APPENDIX II. ELECTRONIC PARAMETERS

The BCS density of states N(0) and the Fermi velocity v_F are calculated for tin and lead. The density of states at the Fermi surface per unit energy per unit volume is

$$D(0) = \frac{S}{4\pi^3\hbar} \overline{\left(\frac{1}{v_F}\right)} \tag{1}$$

where D(0) = 2N(0), S is the area of the Fermi surface (excluding any areas of contact with the zone boundaries), and $\overline{(1/v_F)}$ is the average over the Fermi surface of the reciprocal of the Fermi velocity. The coefficient γ of the electronic specific heat is

$$\gamma = \frac{1}{3} D(0) \pi^2 k_B^{\ 2} \tag{2}$$

where k_B is Boltzmann's constant and can be experessed, using Eq. (1) as

$$\gamma = \frac{k_B^{\ 2} S}{12\pi\hbar} \overline{\left(\frac{1}{v_F}\right)} \ . \tag{3}$$

The Fermi surface area can also be related to the electrical conductivity divided by the electronic mean free path, both averaged over the Fermi surface,

$$\frac{\overline{\sigma}}{\overline{\ell}} = \frac{e^2 S}{12\pi^3\hbar} \ . \tag{4}$$

Equations (3) and (4) yield

$$v_F = \frac{\pi^2 k_B{}^2 \gamma \ell}{e^2 \sigma} \tag{5}$$

if we assume

$$\overline{v}_F = \left[\left(\overline{\frac{1}{v_F}}\right)\right]^{-1} .$$

The experimental values for γ and σ/ℓ are listed in Table I together with the values for N(0) and v_F calculated from Eqs. (2) and (5) respectively. Also included in the table are other quantities of interest: the Debye temperature Θ_D, the resistivity at room temperature ρ, the electronic mean free path ℓ for our films at 4.2K and the bulk coherence lengths ξ_o at T = 0.

The time τ_Θ is the phonon scattering time at a temperature Θ which enters the expression for τ_Q. To obtain τ_Θ we extrapolate from room temperature assuming $\tau \propto T^{-1}$. We have

$$\tau_\Theta = \frac{\ell_\Theta}{v_F} = \frac{\ell_{293}}{v_F} \frac{293}{\Theta} \qquad \text{at } T = 20C .$$

Now

$$\ell_{293} = \frac{\sigma_{293}}{\sigma/\ell}$$

so

$$\tau_\Theta = \frac{\sigma_{293}}{v_F(\sigma/\ell)} \frac{293}{\Theta} .$$

These values are calculated for tin and lead using the values for σ_{293}, Θ, v_F and σ/ℓ from Table I. The results for τ_Θ also appear in Table I.

Table I. Calculation of values for Tin and Lead

Quantity	Units	Tin	Lead	Reference
γ	$\frac{j}{cc\text{-}k^2}$	1.08×10^{-4}	1.62×10^{-4}	ISSP[25]
N(0)	$eV^{-1}cm^{-3}$	1.38×10^{22}	2.07×10^{22}	----
Θ_D	K	200	105	ISSP[26]
σ/ℓ	$\Omega^{-1}\ cm^{-2}$	9.5×10^{10}	9.4×10^{10}	Chambers[27]
v_F	cm/sec	0.65×10^{8}	0.43×10^{8}	----
$\rho(20°C)$	Ω-cm	11.5×10^{-6}	22×10^{-6}	CRC Handbook[28]
$\ell(4.2K)$	Å	2600		----
τ_Θ	sec	2.1×10^{-14}	3.1×10^{-14}	----
ξ_o	Å	2100	800	----

REFERENCES

1. J. Bardeen, L. N. Cooper and J. R. Schrieffer, Phys. Rev. 108, 1175 (1957).
2. A. Rothwarf and B. N. Taylor, Phys. Rev. Letters 19, 27 (1967).
3. K. E. Gray, A. R. Long and C. J. Adkins, Phil. Mag. 20, 273 (1969).
4. C. S. Owen and D. J. Scalapino, Phys. Rev. Letters 28, 1559 (1972).
5. W. H. Parker and W. D. Williams, Phys. Rev. Letters 29, 925 (1972).
6. W. H. Parker, private communication.
7. A. B. Pippard, J. G. Shepherd and D. A. Tindall, Proc. Roy. Soc. A324, 17 (1971).
8. T. J. Rieger, D. J. Scalapino and J. E. Mercereau, Phys. Rev. Letters 27, 1787 (1971).
9. B. D. Josephson, Phys. Lett. 1, 251 (1962).
10. M. Tinkham, Phys. Rev. B6, 1747 (1972).
11. Stuart Bermon, unpublished.
12. W. L. McMillan and P. W. Anderson, Phys. Rev. Letters 16, 85 (1966).
13. P. W. Anderson, J. Phys. Chem. Solids 11, 26 (1959).
14. D. Markowitz and L. P. Kadanoff, Phys. Rev. 131, 563 (1963).
15. J. Clarke, Proc. Roy. Soc. A308, 447 (1969).
16. R. P. Giffard, R. A. Webb and J. C. Wheatley, Journal of Low Temp. Phys. 6, 533 (1973).
17. J. Clarke, I.E.E.E. Proc. 61, 8 (1973).
18. J. R. Waldram, A. B. Pippard and J. Clarke, Phil. Trans. Roy. Soc. A268, 265 (1970).
19. Develco Inc., Superconducting Instruments Division, Mountain View, California 94040.

20. E. Rumbo, Phil. Mag. 19, 689 (1969).

21. J. Clarke, Phys. Rev. Letters 28, 1363 (1972).

22. R. Meservey and B. B. Schwartz, in Superconductivity, edited by R. D. Parks (Marcel Dekker, New York, 1969) p. 141.

23. J. M. Rowell and L. Kopf, Phys. Rev. 137, 907 (1965).

24. R. S. Newbower, Ph.D. thesis, Harvard University, January 1971 (published as a technical report by the Office of Naval Research).

25. Charles Kittel, Introduction to Solid State Physics, Fourth Addition, (John Wiley and Sons, Inc., New York, 1971), p. 254.

26. Charles Kittel, loc. cit., p. 219.

27. R. G. Chambers, Proc. Roy. Soc. 215, 481 (1952).

28. Handbook of Chemistry and Physics, 52nd edition, edited by Robert C. Weast (The Chemical Rubber Co., Cleveland, 1971).

LEGAL NOTICE

This report was prepared as an account of work sponsored by the United States Government. Neither the United States nor the United States Atomic Energy Commission, nor any of their employees, nor any of their contractors, subcontractors, or their employees, makes any warranty, express or implied, or assumes any legal liability or responsibility for the accuracy, completeness or usefulness of any information, apparatus, product or process disclosed, or represents that its use would not infringe privately owned rights.

TECHNICAL INFORMATION DIVISION
LAWRENCE BERKELEY LABORATORY
UNIVERSITY OF CALIFORNIA
BERKELEY, CALIFORNIA 94720